AFRL-AFOSR-UK-TR-2011-0026

Single-cycle Pulse Synthesis by Coherent Superposition of Ultra-broadband Optical Parametric Amplifiers

Giulio Cerullo

Politecnico di Milano
Department of Physics
Piazza Leonardo da Vinci 32
Milano, Italy 20133

EOARD GRANT 09-3101

August 2011

Final Report for 02 September 2009 to 02 September 2010

Air Force Research Laboratory
Air Force Office of Scientific Research
European Office of Aerospace Research and Development
Unit 4515 Box 14, APO AE 09421

REPORT DOCUMENTATION PAGE

Form Approved OMB No. 0704-0188

1. REPORT DATE *(DD-MM-YYYY)*	2. REPORT TYPE	3. DATES COVERED *(From – To)*
01-08-2011	Final Report	2 September 2009 – 02 September 2010

4. TITLE AND SUBTITLE

Single-cycle Pulse Synthesis by Coherent Superposition of Ultra-broadband Optical Parametric Amplifiers

5a. CONTRACT NUMBER

FA8655-09-1-3101

5b. GRANT NUMBER

Grant 09-3101

5c. PROGRAM ELEMENT NUMBER

61102F

6. AUTHOR(S)

Professor Giulio Cerullo

5d. PROJECT NUMBER

5d. TASK NUMBER

5e. WORK UNIT NUMBER

7. PERFORMING ORGANIZATION NAME(S) AND ADDRESS(ES)

Politecnico di Milano
Department of Physics
Piazza Leonardo da Vinci 32
Milano, Italy 20133

8. PERFORMING ORGANIZATION REPORT NUMBER

N/A

9. SPONSORING/MONITORING AGENCY NAME(S) AND ADDRESS(ES)

EOARD
Unit 4515 BOX 14
APO AE 09421

10. SPONSOR/MONITOR'S ACRONYM(S)

AFRL/AFOSR/RSW (EOARD)

11. SPONSOR/MONITOR'S REPORT NUMBER(S)

AFRL-AFOSR-UK-TR-2011-0026

12. DISTRIBUTION/AVAILABILITY STATEMENT

Approved for public release; distribution is unlimited.

13. SUPPLEMENTARY NOTES

14. ABSTRACT

Ultrafast optical science has experienced major breakthroughs in the last years, driven by two main accomplishments: (i) generation of light pulses with duration of just a few cycles of the optical carrier wave; (ii) control of the carrier-envelope phase (CEP) of light pulses, enabling the production of optical waveforms with reproducible electric field.

The generation of extremely short light pulses with controlled CEP allows exploring new frontiers of light-matter interaction, entering the so-called "extreme nonlinear optics regime. In particular, by focusing high-intensity pulses in a noble gas jet, it is possible to produce coherent bursts of XUV radiation by the so-called High Harmonic Generation (HHG) process. Such pulses can have a duration down to approximately 100 as. Attosecond pulses open entirely new perspectives in the study of ultrafast processes relevant to chemical reactions, material science and most importantly the structure and function of biomolecules.

Approaching the pulse duration limit set by the period of the optical carrier wavelength (2-3 fs in the visible to near-IR range) is challenging because of the requirement to control the pulse spectral amplitude and phase over an ultrabroad bandwidth. It has long been recognized that (sub)single-cycle optical pulses may be generated through phase coherent superposition of several independent few-cycle laser pulses tuned to different carrier frequencies. A great deal of experimental work has been carried out on coherent pulse synthesis from two separate broadband mode-locked laser oscillators; such task is however very demanding because it requires synchronization of two laser cavities to within a fraction of the carrier period (100-200 as). In addition, synchronization of two oscillators allows generating only limited pulse energies (of the order of 1 nJ), which are not sufficient to drive the HHG process. So far no experimental work has been performed on the synchronization of high-energy broadband light pulses.

15. SUBJECT TERMS

EOARD, Non-linear Optics, Optical parametric oscillators

16. SECURITY CLASSIFICATION OF:			17. LIMITATION OF ABSTRACT	18, NUMBER OF PAGES	19a. NAME OF RESPONSIBLE PERSON
a. REPORT	b. ABSTRACT	c. THIS PAGE			A. GAVRIELIDES
UNCLAS	UNCLAS	UNCLAS	SAR	45	19b. TELEPHONE NUMBER *(Include area code)* +44 (0)1895 616205

Project AFOSR FA8655-09-1-3101.

Single-cycle pulse synthesis by coherent superposition of ultra-broadband optical parametric amplifiers

Final Report

TABLE OF CONTENTS

Summary

In the fourth reporting period we have extended and concluded the theoretical analysis of noise propagation in OPCPAs, and gained useful information for the optimization of OPCPA design parameters. From the experimental side, we have optimized two set-ups for coherent pulse synthesis and CEP-stable pulse generation.

The main results obtained are summarized in the following:

Simulations of noise evolution in OPCPAs

The quantum-mechanically consistent numerical model detailed in the previous reports allowed us to conclude the investigation of the dynamics of superfluorescence growth in a realistic high-gain OPCPA. Since the model can simulate also the saturation stage of amplification, our investigation for the first time captured all dynamics of a quantum-noise-contaminated OPCPA, addressing the important practical issues of signal energy stability and pulse contrast. The different evolution dynamics of these quantities were analyzed throughout the amplification process in three operating conditions, characterized by different chirps of the input seed. We find maximization of the efficiency-bandwidth product is correlated to the noise contamination; in addition, while amplifier saturation improves the signal's shot-to-shot energy stability, it does not necessarily improve the pulse contrast. Knowledge of these dynamics increases our fundamental understanding of quantum noise in parametric amplification; it also provides important insight for the optimization of OPCPA systems applied to the study of strong-field laser physics.

Synthesis from two-stage parametric amplification

In order to generate the gap-free phase-stable ultrabroadband WLC required by this task, we have first developed a two-stage IR-OPA. This setup removes the spectral gap at 800 nm typically arising after spectral broadening the fundamental frequency of a Ti:sapphire laser. The two-stage IR-OPA provides signal/idler pulses at wavelengths longer than 1.3 μm, which are then broadened in a YAG or sapphire plate. The WLC is split in two and used to seed simultaneously the visible NOPA and the degenerate OPA, which are then separately compressed using chirped mirrors to nearly TL duration. The two pulses are combined using a broadband beam splitter and their relative CEP and delay is monitored by spectral interferometry. Preliminary results demonstrated that combination of the OPA pulses allows obtaining a broadband pulse extending from 550 to 1000 nm, corresponding to a transform-limited duration of 4 fs.

Sub-cycle pulse synthesis from two OPCPAs

We have realized a waveform synthesis scheme which is able to combine high-energy, few-cycle optical pulses from multi-color OPCPAs. The system generates a sub-cycle waveform with a

spectrum spanning close to two octaves and 15-μJ pulse energy. This source can be applied to the direct generation of isolated soft-x-ray pulse by HHG, eliminating the need for gating techniques or spectral filtering. The system is capable of stabilizing and controlling all independent parameters that define the synthesized electric-field waveform, such as the absolute phase and the relative delay of the two pulses.

Introduction

The aim of the project is to develop two (or more) ultra-broadband CEP-stable Optical Parametric Amplifiers (OPAs) and coherently combine their outputs in order to synthesize high energy (sub)single-cycle pulses with controlled electric field profile.

OPAs are devices which exploit second order optical nonlinearity in order to efficiently transfer the energy of a fixed frequency "pump" pulse to a broadly tunable weak "signal" pulse. To achieve efficient energy transfer, the so-called "phase matching" condition between the interacting waves must be satisfied. Under appropriate conditions, phase matching can be achieved over a broad frequency range, thus turning OPAs into ultra-broadband amplifiers and allowing the generation of tunable few-optical-cycle light pulses.

Broad gain bandwidth in an OPA is achieved when the group velocities of signal and idler are matched [1]; this condition is satisfied either in the case of type I phase matching at degeneracy, or in the non-collinear OPA (NOPA), in which the idler group velocity is projected along the signal propagation direction. Using these concepts, a variety of broadband OPA schemes, pumped by either the fundamental frequency (FF) or by the second harmonic (SH) of Ti:Sapphire and seeded by white light continuum (WLC), have been demonstrated. The SH-pumped NOPA in the visible [2-4], the FF-pumped NOPA in the near-IR [5, 6] and the FF-pumped near-IR degenerate OPA [7] allow to cover nearly continuously the wavelength range from 500 to 2 μm.

The goals of this project are: (i) to develop two broadband OPAs for the amplification of CEP-stable seed light in a broad wavelength range, from 500 nm to 2 m; (ii) to coherently combine these OPAs in order to synthesize a single-cycle optical pulses with CEP control, *i.e.*, with a precisely defined electric field waveform [8]. Such CEP-stable single-cycle pulses will be used to drive strong-field processes such as high-harmonic generation (HHG), which has recently led to efficient generation of isolated attosecond pulses, with duration as short as 80-as in the XUV range [9].

In order to fulfill the aims of the project, the following two tasks have been addressed in the fourth period of the project:

Task 1 - Generation of few-optical-cycle CEP stable pulses from OPAs

Simulations of noise evolution in OPCPAs

Our pulse synthesis experiments require the coherent combination of pulses generated by parametric amplification (OPAs and OPCPAs). The unusual phenomena associated with quantum noise contamination in an OPCPA, observed but heretofore not well understood, are the concern of this part of the project. While OPCPAs are immune from amplified spontaneous emission, they are on the other hand prone to another parasitic effect with evolution dynamics that are not well understood in this geometry, namely parametric superfluorescence (PSF), i.e., parametric amplification of the vacuum or quantum noise due to two-photon spontaneous emission from a virtual level excited by the pump field [10]. Previous experimental results have shown that the presence of PSF results in an amplified signal field with two apparent macroscopic components: a coherent pulse with well defined temporal chirp that matches that of the seed pulse, and which is dechirped in the compression stage to generate a transform-limited pulse, and an incoherent pedestal with stochastic phase statistics similar to that of spontaneous parametric generation, which cannot be recompressed. Henceforth, we refer to these phenomenological components observed at the output of an OPCPA as the *coherent pulse* and *incoherent pedestal*, respectively. Here we will report on the numerical study of the incoherent pedestal; the aim of the study is to provide a guideline for the project and realization of OPCPA with optimized signal-to-noise ratios.

Task 2 - Coherent pulse synthesis

We have implemented two schemes for the synthesis of nearly single cycle pulses: coherent combination of two broadband OPAs (performed in Milano) and of two high-energy OPCPAs in the near and mid-IR (performed at MIT). The first scheme offers the advantage of a clean gap-free spectrum, allowing the generation of pulses without satellite lobes, but has currently limited output energy; the second scheme, on the other hand, has the advantage of energy scalability but presents some side-lobes due to a gap in the synthesized spectrum.

Synthesis from two-stage optical parametric amplification

In the previous report we introduced three possible schemes for the synthesis of few-cycle pulses, based on the combination of two ultrabroadband OPAs powered by the same Ti:Sapphire laser. OPAs are very versatile and efficient tools for the generation of few-cycle optical pulses. In this phase of the project, we are developing the first of the proposed schemes, based on the coherent combination of two separate OPAs operating in parallel.

Sub-cycle pulse synthesis from two OPCPAs

We demonstrate a new approach, based on coherent wavelength multiplexing of ultra-broadband OPCPAs, for the generation of fully controlled high-energy sub-cycle optical waveforms with spectra spanning close to two octaves. Such pulses can be used to efficiently generate isolated attosecond pulses without the use of gating techniques [11]. The system coherently combines two CEP-controlled, few-cycle pulses obtained from different OPCPAs: 1) a near infrared (NIR)-OPCPA, producing 25-μJ, 9-fs pulses centered at 870 nm; and 2) a short-wavelength infrared (SWIR)-OPCPA, producing 25-μJ, 24-fs pulses centered at 2.15 μm.

Methods, assumptions and Procedures

Task 1 - Generation of few-optical-cycle CEP stable pulses from OPAs

Simulations of noise evolution in OPCPAs

The quantum-mechanically consistent numerical model already introduced in the previous reports was further optimized and applied to evaluate the nature of noise in OPCPAs. Such noise arises from parametric superfluorescence, *i.e.* amplification of vacuum fluctuations. For the numerical description of this process, we focus on an OPCPA seeded by the initial quantum noise field and a chirped signal field. The nonlinear quantum system dynamics can be described by a quasi-probability distribution, such as the Wigner distribution (WD) [12]. For linear systems the evolution equation for the WD is equivalent to a classical Fokker-Planck equation, and is thus also equivalent to a stochastic process involving classical noise sources, resulting in a semiclassical picture of the quantum process. This correspondence has been exploited in numerical studies of PSF, OPA, and optical parametric oscillation in their linear regimes [13, 14]. The Fokker-Planck approximation also holds for the case of weak nonlinearities, and the nonlinear quantum system dynamics can still be extracted accurately from stochastic Langevin equations [15, 16], an approach used earlier to study the quantum noise in parametric amplifiers used for squeezed light generation [17, 18]. These stochastic equations have a deterministic component equal to the Heisenberg equations of motion for the field operators and are complemented by relaxation terms and associated noise terms. For the case of a lossless OPA process, fluctuations stem solely from the quantum mechanical uncertainty in the input fields. Knowledge of a quasi-probability distribution allows computation of all expectation values of quantum mechanical observables, and for the case of the WD and its associated stochastic process, computed expectation values correspond to quantum mechanical expectation values of symmetrically ordered field operators [12]. In practice, we simulate the evolution of noise in an OPCPA by numerically solving the coupled nonlinear equations of parametric amplification in the spectral domain, accounting for linear dispersion to all orders [19, 20]. Our 1-D plane wave model includes all longitudinal modes, *m*, and their associated noise. In the frequency domain, at any mode frequency, ω_m, the corresponding

component of the initial signal, idler, or pump electric field is represented by a complex stochastic phasor, $A_m(0)=B_m+n_m$. B_m is the deterministic component of the field, and is set to 0 in the case of the idler; n_m is a zero-mean, stochastic phasor representing the independent fluctuations of the field. The initial fields then follow the conventional interaction and propagation equations of the OPCPA process. Note that fluctuations are included for each of the signal and idler fields. Real and imaginary components of n_m are taken as uncorrelated Gaussian distributions [13] with variance $\sigma_m^2 \propto \omega_m$.

By virtue of the model's adherence to quantum mechanics even in the saturation stage of amplification, our investigation captures for the first time the saturation dynamics of quantum-noise-contaminated OPA, a problem of general interest in the fields of quantum and nonlinear optics, both theoretically and experimentally.

We have simulated the broadband 2-μm OPCPA which has been developed in the labs at MIT. The system employs a periodically-poled lithium tantalate crystal pumped by a 9-ps Gaussian pulse at 1.047 μm and seeded by a broadband pulse at 2.094 μm, for operation around degeneracy. The seed spectrum has FWHM bandwidth of 69 THz, which well matches the 15-fs phase-matching bandwidth of the amplifier. We investigated a high-gain amplifier stage, where the pump-to-signal energy ratio is $E_p/E_s=10^6$. The seed field was chirped respectively to 1.0-ps, 7.3-ps, and 10.5-ps durations; these configurations are correspondingly labeled I: "low chirp", II: "optimal chirp", III: "high chirp".

We then present an analysis of the evolution of SNR across the propagation axis that allows us to identify changes in SNR which occur during different stages of amplification: *initial growth*, *saturation*, and *over-saturation*, using a one-dimensional OPCPA model that considers all longitudinal modes and associated noise.

Task 2 - Coherent pulse synthesis

Pulse synthesis from two-stage optical parametric amplification

This approach was followed in Milano and aimed at the generation of a gap-free nearly single-cycle pulse by coherent synthesis of two OPAs. In the last phase of the project, we have developed the first of the schemes proposed in section "***Methods, assumptions and Procedures***"of the third report, based on two separate OPAs operating in parallel. Among the three proposed schemes, we selected the approach based on two parallel and independent OPAs for the amplification of an ultrabroadband seed extending from 500 to 1000 nm [Figure 1(a)]. The OPAs gain bandwidths cover two partially overlapping spectral portions of this region, allowing the generation of ultrabroadband pulses without detrimental gaps in the spectrum [Figure 1(b)].

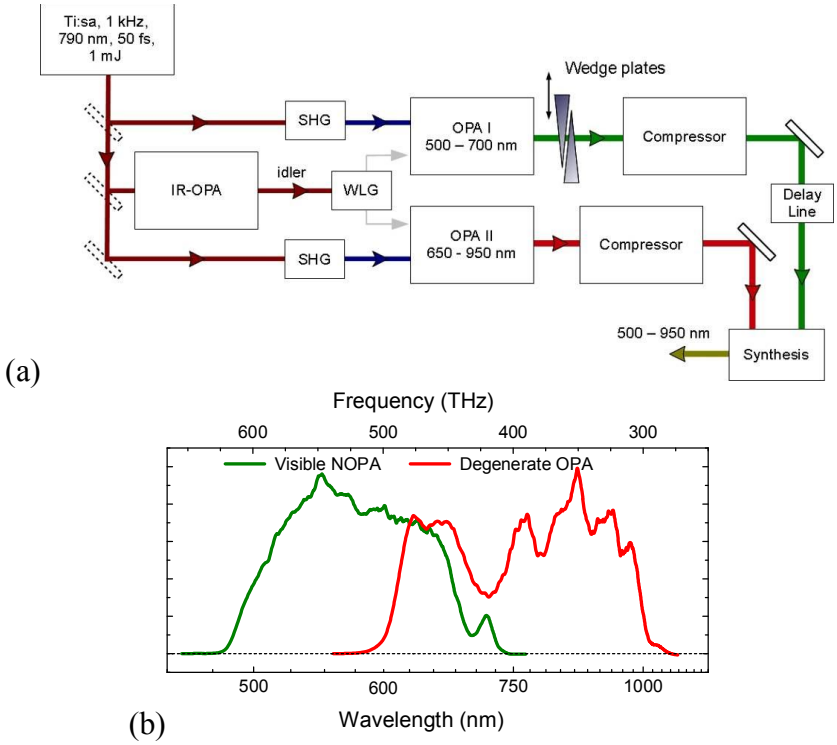

Figure 1: (a) setup for separate optical parametric amplification, compression and coherent combination of visible and near-infrared pulses. SHG: second harmonic generation; WLG: white light generation. (b) Spectra from a typical OPA I (visible NOPA) and OPA II (degenerate OPA).

The three building blocks of this approach are:

- The two-stage IR OPA, powered by the fundamental of our laser source at 800 nm and seeded by the IR portion of a WLC produced in sapphire. The IR light arising from this system is then used to generate a supercontinuum by self-phase-modulation in a YAG plate. The supercontinuum, ranging from 500 to 1000 nm.; will seed the two OPAs described in the following.
- The SH-pumped non-collinear OPA (NOPA), which amplifies broadband visible pulses in the 500-700 nm range [21] (see figure 1 (b));
- The SH-pumped OPA at degeneracy [22], detailed in the First Interim Report of the project; this OPA provides 7-fs pulses in the 700-1000 nm range (see figure 1 (b)).

The first block aims at the generation of the phase-stable broadband white light; to this end, a great effort has been devoted to the realization of a reliable set-up, driven by the fundamental beam of our laser and based on a two-stage IR OPA. The two OPA crystals employ a type II configuration, which provides a stable narrow-band amplification. The first OPA is tuned at 1500 nm and generates the idler at 1700 nm. Since amplification arises from the interaction between phase-locked signal and pump pulses, the idler is self-phase stabilized (23, 24). The phase-stable idler pulse is then amplified in the second stage, driven to saturation and designed in order to optimize the idler energy stability. The resulting amplified beam is focused into a YAG plate for the generation of the ultrabroadband supercontinuum. The WLC is split in two and used to seed simultaneously the visible NOPA and the

degenerate OPA, which are then separately compressed using chirped mirrors to nearly TL duration. The two pulses are combined using a broadband beam splitter and their relative CEP and delay is locked using a nonlinear correlator.

Sub-cycle pulse synthesis from two OPCPAs

This approach was followed at MIT, in collaboration with Milano, and aimed at the generation of energy scalable sub-cycle optical waveforms by the coherent synthesis of two OPCPAs. Figure 2 shows a schematic of the system. It starts with an actively CEP-stabilized octave-spanning Ti:sapphire oscillator. The oscillator's repetition rate serves as the master clock for the full system, and the 1047-nm component feeds a 1-kHz Nd:YLF chirped pulse amplifier (CPA) system to pump the OPCPAs. The oscillator output directly seeds the NIR-OPCPA while its spectral edges (centered at 650 nm and 930 nm) undergo intrapulse difference-frequency generation (DFG) to produce a pulse at 2.15 μm that seeds the SWIR-OPCPA. Using a single oscillator as front-end for the entire system ensures the coherence of the two OPCPA pulses to within environmental fluctuations and drifts on subsequent beam paths. The designs of the OPCPAs follow the guidelines described in previous studies [25, 26] for simultaneously optimizing energy conversion, amplification bandwidth, and signal-to-noise ratio.

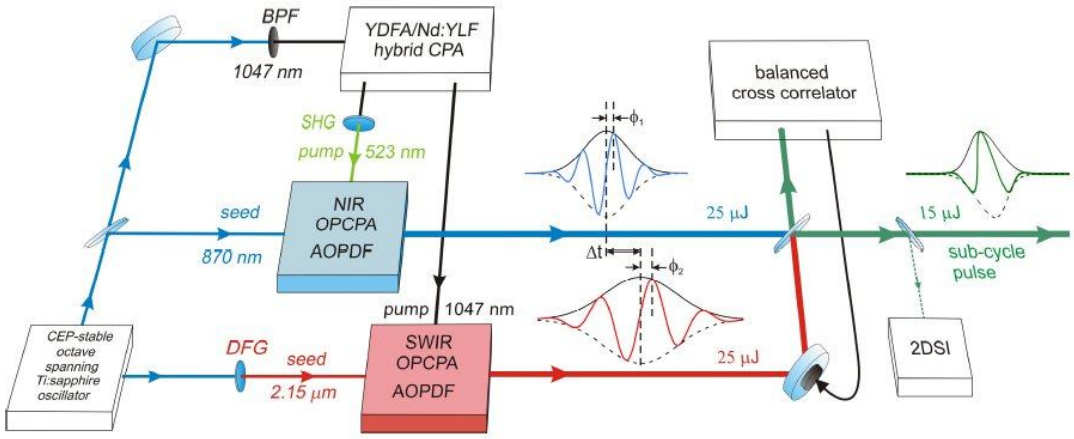

Figure 2: Two CEP-stabilized, few-cycle OPCPAs centered at different wavelengths are combined based on the concept of coherent wavelength multiplexing to produce 15-μJ, 0.6-cycle pulses at 1-kHz repetition rate. Full control over the optical phase allows for any optical waveform given the amplified spectrum. YDFA: Ytterbium-doped fiber amplifier; BPF: bandpass filter.

Of note, the inclusion of an acoustooptic programmable dispersive filter (AOPDF) in each OPCPA allows independent spectral phase and amplitude adjustment of each pulse, enabling control and optimization of the synthesized waveform. Outputs from the two OPCPAs are combined in a broadband neutral beam splitter. Besides the spectral phases (controlled by the AOPDFs), three other independent parameters (see Fig. 2) determine the synthesized electric-field waveform: the CEP of the

NIR-OPCPA pulse (φ_1), the CEP of the SWIR-OPCPA pulse (φ_2), and the relative timing between the two OPCPA pulses (Δt).

Precise stabilization of these three parameters is required for coherent synthesis of the two OPCPA pulses, and subsequent control of each parameter allows precise waveform shaping. While the CEP of the SWIR-OPCPA is passively stabilized due to the intrapulse DFG process used to produce its seed, an active feedback loop on the oscillator is implemented to ensure the CEP stability of the NIR-OPCPA. A feedback loop based on a balanced cross-correlator (BCC) [27] is implemented to synchronize the two pulses, allowing attosecond-precision relative timing stability. A BCC is the optical equivalent of a balanced microwave phase detector, and is particularly suitable for timing drift measurements with sub-cycle precision because the balanced detection cancels the amplitude noise. Once the BCC-assisted feedback loop stabilizes the relative timing between the two OPCPA pulses, a two-dimensional spectral-shearing interferometer (2DSI) [28] is used to measure the frequency-dependent group-delay of the synthesized pulse. A 2DSI is a variation of spectral-shearing interferometry, and it circumvents the challenge of calibrating interferometer delay by encoding the group-delay information in pure sinusoidal fringes along a wavelength independent axis, obtained by scanning the relative phase of the two spectrally sheared components over a few NIR periods.

Results and discussion

Task 1 - Generation of few-optical-cycle CEP stable pulses from OPAs

Simulations of noise evolution in OPCPAs

Integration of the described nonlinear equations allowed to follow the fluctuating fields during amplification. A graphical representation of the statistics of signal field is given in Fig. 3 (a) and (b), where we show B_m (vectors), and A_m and n_m (scatter) for three modes ω_m of the signal field. The simulations refer to an ultra-broadband OPCPA system known to be sensitive to PSF [25, 29,]. The amplifier, pumped by a 9-ps FWHM Gaussian pulse at 1.047 μm and seeded by a broadband (69-THz FWHM) pulse at 2.094 μm for operation around degeneracy, uses a 3-mm long PPSLT crystal with poling period $\Lambda = 31.2\mu m$. These parameters are close to the experimental conditions of Ref. [25]. In this example, the pump-to-seed energy ratio is 10^6. The variances σ_m^2 of the noise field are determined by the quantum fluctuations due to the longitudinal modes of the 100-ps-long simulation window. This number is further increased by a factor equal to the number of transverse modes amplified assuming a pump beam of 100-μm radius in the 3-mm long crystal, which is estimated as about 25. We note that this choice results in a calculated amplified pulse contrast that closely matches that observed in equivalent experiments [25]. For each configuration, we evaluated 50 independent trajectories triggered by uncorrelated noise fields. The averages taken over this ensemble of classical

solutions correspond to quantum-mechanical expectation values [30]. The results of a batch of simulations are depicted in Fig. 3(c). The incoherent nature of the amplified noise is evidenced in panel (d), representing the same fields after compression.

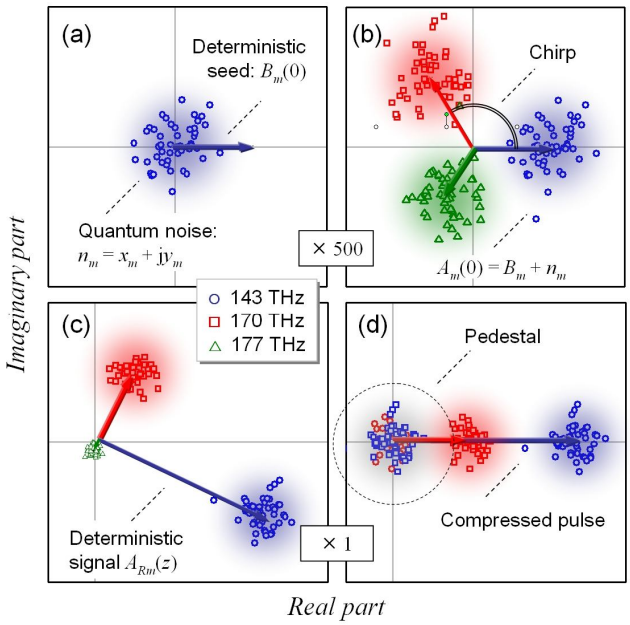

Figure 3 (a) Schematic representation of the deterministic part (arrow) and 50 stochastic components (circles) of a field mode. (b) Initial signal field distribution (scatter), evaluated at three modes of frequency ω_m, experiencing respectively the highest gain G_0, $G_0/2$ and $G_0/10$ and separated by a phase shift imparted by the chirp. (c) Depiction of the same modes after amplification and (d) after compression; pedestal fields deduced after subtracting the deterministic components are indicated in the dashed circle. All data refer to configuration II. Panels (a) and (b) are magnified 500 times with respect to (c) and (d).

The role and amplitude of noise during amplification along propagation distance z was evaluated by the two approaches introduced in previous reports and here summarized: in a first approach, we calculated the signal-to-noise ratio (SNR) as the ratio between the mean and the standard deviation of the seed pulse energy, $\langle E(z)\rangle/\Delta E(z)$; a second figure of merit is the Signal-to-Pedestal Ratio (SPR), which directly compares the average energy of the *incoherent pedestal* with the *coherent pulse*. It is important to stress that SPR is accessible only by numerical approaches, since it cannot be experimentally measured and the two contributions cannot be separated. Analysis of these figures during amplification allows deducing many properties of the noise added to the amplifier in the presence of pump depletion and as a function of the amplification parameters, such as signal chirp and pump peak intensity. In particular we evaluated 3 configurations, which correspond to: an under-chirped amplifier, with maximum amplified signal bandwidth but limited conversion efficiency (Configuration I); an amplifier chirped for maximum efficiency-bandwidth product (Configuration II); and an over-chirped amplifier (Configuration III), with excellent conversion efficiency but significant spectral narrowing. Mean and standard deviation of seed and idler pulse energies, together with the pedestal energy, are given in Fig. 4. The two panels allow comparing configurations I and II, showing that the pedestal dramatically depends on amplification parameters, which thus have to be

carefully tuned in order to minimize detrimental tails in the signal temporal profile.

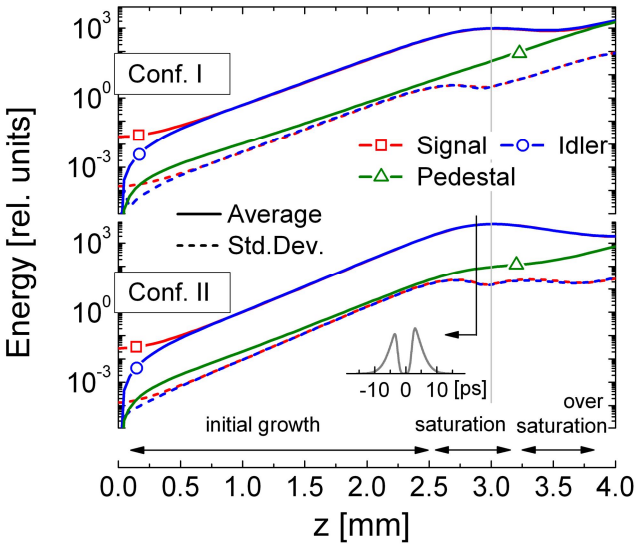

Figure 4: Evolution of energy mean and standard deviation for signal and idler; the energy growth of the pedestal mean is also given. In the case of configuration II we indicate the coordinate at which the pump peak is fully depleted (see inset). Trends calculated for configuration III (not shown) are comparable to the ones of configuration II

Evaluation of SNR and SPR shows that the two approaches for noise estimation follow different behaviors: in particular the low-chirp regime (configuration I), exhibits a poor SPR, due to a strong pedestal component. This can be explained by the fact that energy fluctuations $\Delta E(z)$ and pedestal energy $\langle E_P(z) \rangle$ are not directly correlated: saturation generally mitigates energy fluctuations, also when this energy mainly comes from noise. In this sense, the low-chirp configuration is particularly sensitive because the seed pulse efficiently extracts all the energy from the peak of the pump, but the rest of the pump energy is transferred to the pedestal. The effect of the pedestal is confirmed by comparing the temporal shape of the pulses after compression: the uncoherent pedestal is only marginally affected by compression, thus giving rise to a strong plateau with the same duration of the pump beam. This long pulse has detrimental effects for those processes requiring a very high pulse contrast.

Task 2 - Coherent pulse synthesis

Synthesis from two-stage optical parametric amplification

The first building block of this scheme required the preliminary implementation of a two-stage IR OPA for the generation of self-phase stabilized, high-energy pulses; such pulses will then drive supercontinuum generation in a thick YAG plate. A detailed schematic of the setup is shown in figure 5: a small fraction of the driving pulse at 800 nm is spectrally broadened in a 2-mm thick sapphire plate; the IR components of this supercontinuum are then amplified in an IR OPA based on 3-mm

thick BBO crystal cut for type II operation. We chose to propagate both pump and seed with extraordinary (horizontal) polarization in order to generate idler photons with ordinary (vertical) polarization, as required by the subsequent stages. In addition, type II was chosen because it provides narrowband amplification and exhibits higher gain thanks to the trapping effect induced by the favourable group-velocity mismatches. In this case, signal and idler pulses walk in opposite direction with respect to the pump, so that a nonlinear interaction mechanism localizes them under the pump pulse and the gain grows exponentially even for crystal lengths well in excess of the pulse splitting length. To qualitatively understand this trapping effect, we can consider the situation in which the signal pulse has moved slightly to the front and the idler pulse to the back of the pump pulse: during the parametric process, the signal pulse generates idler photons, which move to the back, i.e., toward the peak of the pump; on the other hand the idler pulse generates signal photons which in turn move to the front, again toward the peak of the pump.

The first OPA operates at 1500 nm signal wavelength, corresponding to idler pulses at 1.7 microns wavelength. Typical signal+idler energy is of the order of 5 μJ. After rejecting the residual pump pulse by means of a long-pas filter, and the signal thanks to a polarizer, the idler pulses are sent to the second stage for further amplification. This stage employs a 4-mm thick BBO crystal, and is pumped by 800-nm pulses with 150 μJ energy.

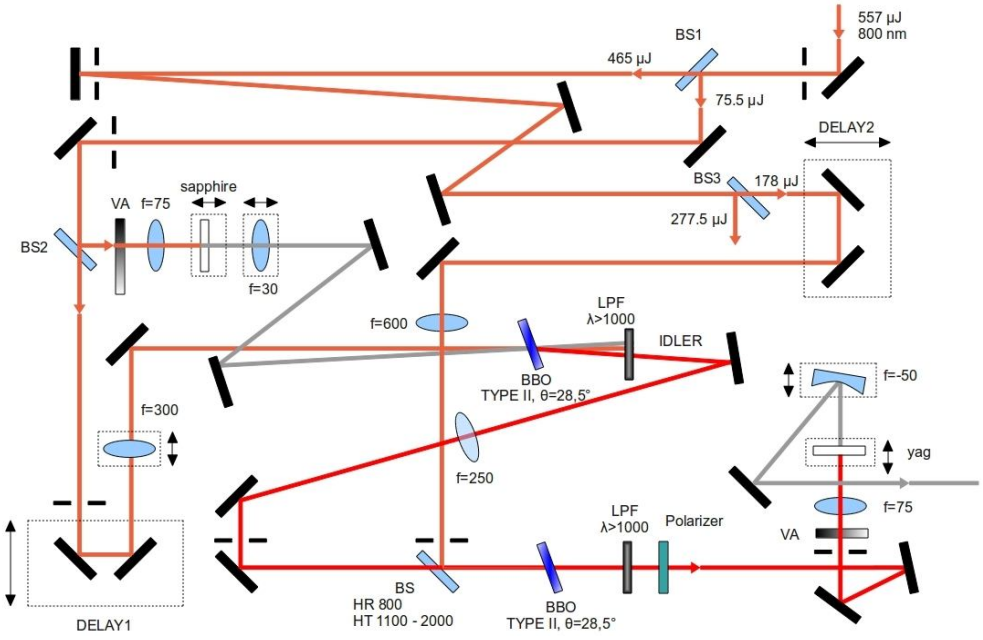

Figure 5: Detailed experimental setup of the two-stage IR OPA for the generation of gap-free supercontinuum light.

Signal and idler spectra from the two-stage OPA are shown in Fig. 6 (a). Note that here Idler and Signal are named after the first stage, and that the second stage is tuned in order to amplify the idler light (black solid line). A small non-collinear angle between pump and idler in the second stage allows spatial separation of the amplifed idler from the residual pump and signal photons, which may be detrimental for the generation of a phase-stable supercontinuum. The stage provides vertically-

polarized, 25-μJ idler pulses, with energy fluctuation of the order of 2%. Such pulses are then focused in a 3-mm thick sapphire plate for spectral broadening thanks to self-phase modulation. The resulting supercontinuum is shown as blue solid line in Fig. 6(b); this spectrum covers the amplification bandwidth of the subsequent visible NOPA and the degenerate 800-nm OPA, as shown by the green and red solid line reported in the same panel.

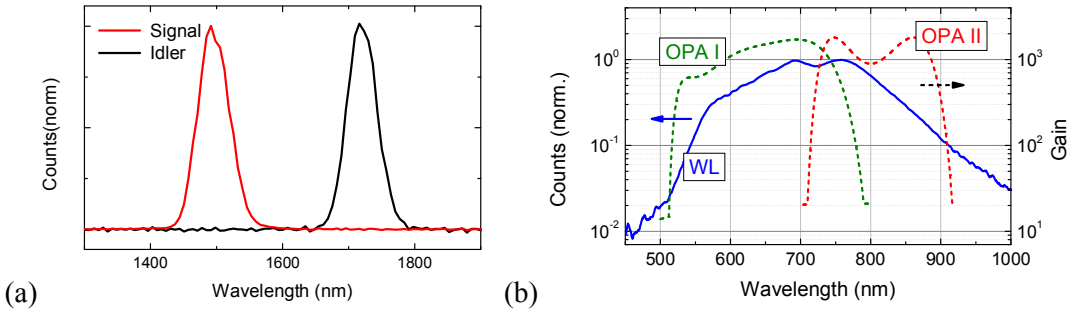

Figure 6: (a) signal and idler spectra from the second stage of the double-OPA setup. The idler pulses, with vertical polarization, drive the supercontinuum generation in a 4-mm thick YAG plate. (b) Spectrum of the gap-free supercontinuum (blue line) generated in the YAG plate, compared to the gain of the visible and infrared OPAs that will be employed for its amplification.

The supercontinum is subsequently split into two identical replicas by a broadband ultrathin beamsplitter, and synchronized with the visible and IR OPAs for amplification. The visible NOPA is pumped by the second harmonic of the 800-nm beam, provided by frequency doubling in a 4-mm thick BBO crystal. Such a thick BBO crystal was chosen in order to narrow the SH spectrum and increase its pulse duration to facilitate its overlap with the strongly chirped seed. Amplification provides 1-μJ visible pulses extending from 500 nm to 750 nm (see Fig. 7(a), green solid line); temporal compression is obtained by 12 bounces onto specially designed Double Chirped Mirrors (DCMs).

The degenerate OPA has a similar design, the only difference being the angle between pump and seed and the required bounces on the DCMs. Degenerate OPA requires that the seed propagates collinearly with the pump; here a small non-collinear angle allows to fulfill this condition and to separate the amplified signal from the spectrally overlapped idler. Compression is achieved by onto DCMs, designed to compensate dispersion from 650 nm to 1.1 microns; thanks to their capability to introduce strong negative dispersion, and to a smaller material dispersion in the infrared spectral range than in the visible, only two bounces are sufficient to obtain a duration close to the TL.

To ensure good spatial overlap of the collimated beams, the two OPAs are designed in order to employ the same focal lengths and to propagate the beams for the same distances. The two amplified pulses are then synchronized by a delay line equipped with a piezoelectric actuator, and collinearly combined by a second ultrathin beam-splitter. A gap-free spectrum arising from the combination of the two pulses is shown in Fig. 7(a); it supports sub-4 fs pulse duration. The pulse energy of the

synthesized pulse is 500-800 nJ.

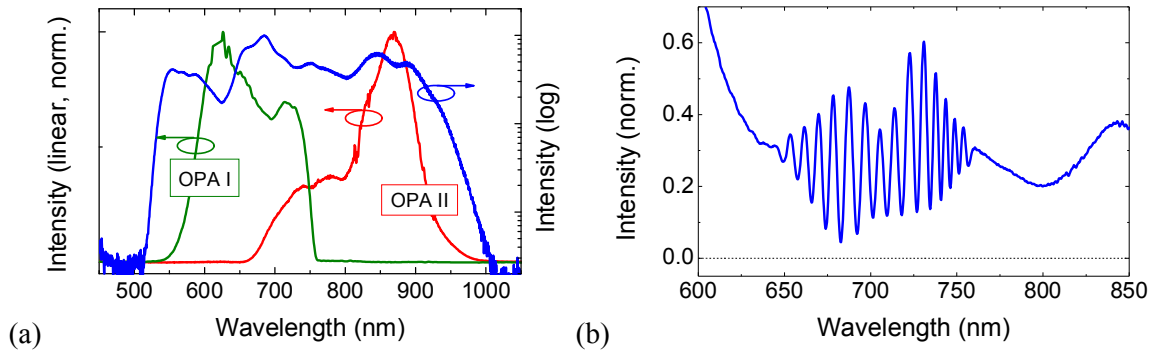

Figure 7: (a) Spectrum of the OPAs light and of the synthesized pulses (blue line, log scale); the total spectrum supports sub-4 fs pulse duration. (b) Interference fringes arising when the pulses are combined with 200-fs delay.

The last challenging step of the pulse synthesis is the coherent combination of the two pulses, which calls for careful control of their relative delay and phase. Thanks to the spectral overlap of the two beams, we could directly use spectral interferometry to characterize their delay fluctuations (see Fig. 7(b)); for this purpose, the delay between the unlocked pulses was increased to about 200 fs and the spectral fringes were monitored for one minute, giving slow delay fluctuations with rms of the order of 3 fs. When seeded with CEP stable continua, we plan to lock the relative delay of the pulses by using the balanced nonlinear cross-correlator (BCC) [27] shown in Fig. 8, which allows attosecond-precision relative timing stability thanks to the capability of the balanced detection scheme to cancel the amplitude noise [31].

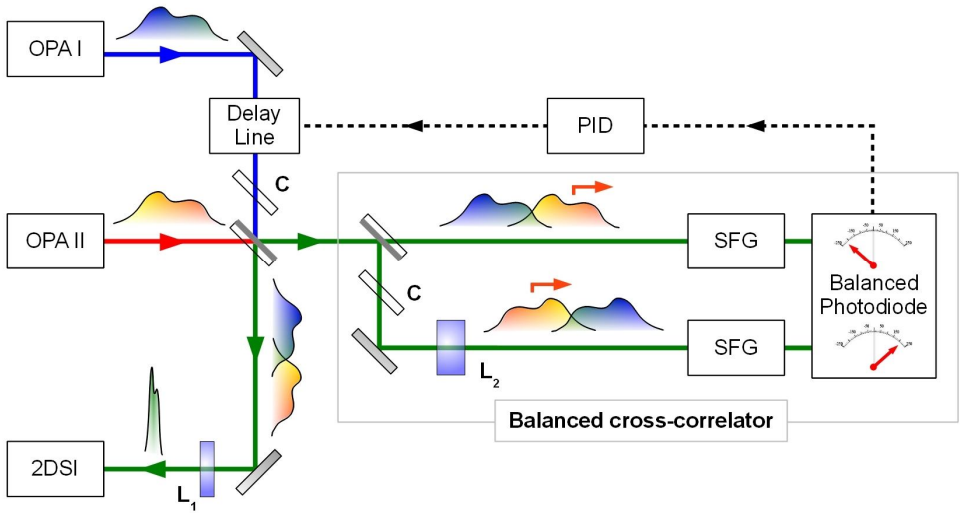

Figure 8: Balanced cross-correlator (BCC) used to lock the delay of the pulses from OPA I and OPA II. $L_{1,2}$: Fused silica plates to obtain respectively compression and positive chirp; C: compensation plates to match the dispersion of all arms; SFG: sum-frequency generation stages; PID: low-pass filter and control module for the feedback on the delay line. The cartoon displays the effects of a delay on the OPA II pulse.

Sub-cycle pulse synthesis from two OPCPAs

In the following we present the results obtained at MIT, in collaboration with Milano, on the generation of sub-cycle optical waveforms by coherent synthesis of two OPCPAs. The overall spectrum spans over 1.8 octaves (green lines in Fig. 9(a)) and the energy of the synthesized pulse is 15 μJ. Due to the gap in the center of the optical spectrum, raw data of a 2DSI measurement is segmented into two parts and then presented. Figures 9(d) and 9(e) demonstrate the CEP stability of the two individual pulses, with r.m.s. fluctuations as low as 135 mrad and 127 mrad, respectively. Figure 9(f) characterizes the relative timing stability. With the feedback control of the SWIR-OPCPA's path length over a bandwidth of 30 Hz, the relative timing drift is reduced to 250 as, less than 5% of the oscillation period of the SWIR-OPCPA (7.2 fs). Figures 9(b) and 9(c) show the raw data of a 2DSI measurement while Fig. 9(a) plots (black lines) the extracted frequency-dependent group-delay of the synthesized pulse, which is the derivative of the spectral phase with respect to frequency. The 2DSI measurement shows that the two OPCPA pulses are temporally overlapped and each is well compressed to within 10% of its transform-limited pulse duration. In our system, the CEPs can be varied by slight tuning of any dispersive element, including the AOPDFs. The values of the CEP will be determined automatically *in situ* when strong-field experiments are conducted and hence CEP tunability is sufficient from an experimental point of view.

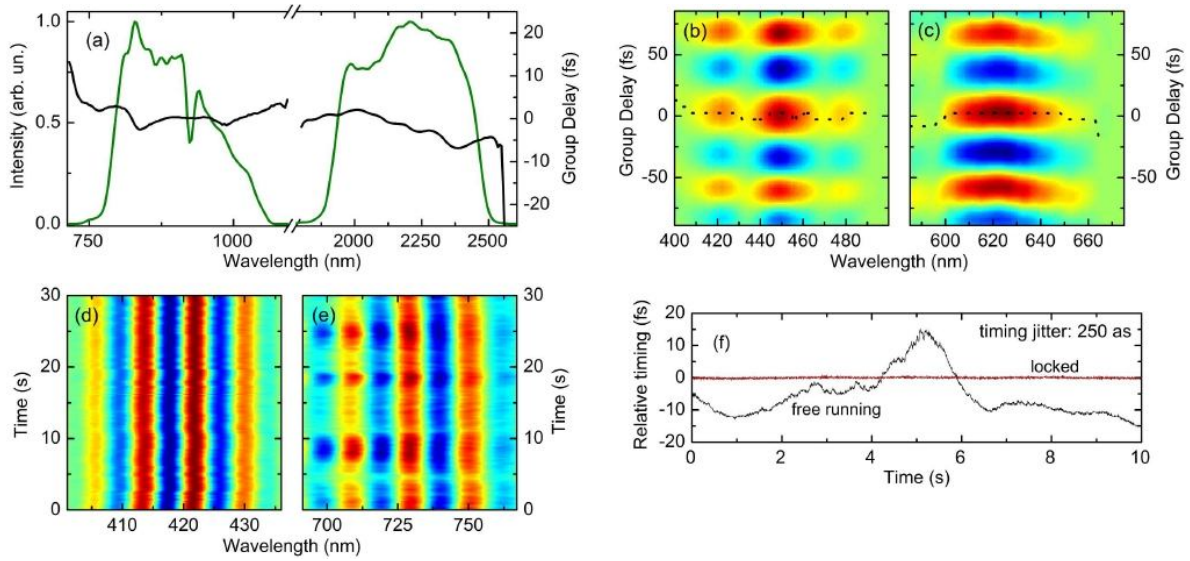

Figure 9 (a) Optical spectrum and frequency-dependent group-delay of the synthesized pulses. The overall spectrum spans over 1.8 octaves and supports sub-cycle pulses. (b) is the 2DSI trace for the NIR-OPCPA and (c) is that for the SWIR-OPCPA. CEP stabilities are verified using nonlinear interferograms. (d) f-2f interferogram, measuring 135 mrad rms (5-shot integration) CEP fluctuations for the NIR-OPCPA. (e) f-3f interferogram, measuring 127 mrad rms (5-shot integration) CEP fluctuations for the SWIR-OPCPA. The BCC-assisted feedback loop guarantees the relative timing stability and (f) shows BCC measurements of the free-running system (black) and the closed-loop system (red). The closed-loop system ensures a relative timing drift of 250 as. The relative timing drift could be reduced even further to 100 as if the feedback bandwidth were extended to 100 Hz.

Figure 10 plots a synthesized electric-field waveform and intensity profile assuming the CEPs (φ_1=650mrad, φ_2=-750mrad) optimal for achieving the shortest high field transient, which lasts only 0.8 cycles (amplitude FWHM) of the carrier (centroid) frequency (λ_c = 1.26 μm). The lower inset of Fig. 10(a) clearly shows that the synthesized electric-field waveform is non-sinusoidal and the main feature lasts less than an optical cycle. As an example of waveform shaping made possible by tuning parameters of our system, Figs. 10(b) and 10(c) show two waveforms as the CEP and the relative timing are changed. Due to the large gap in the combined spectrum, there are wings 4.8 fs from the central peak as shown in Fig. 10(a). These wings should be absent in the approach follwed in Milano, since the synthesized pulses are spectrally overlapped, thus generating a gap-free spectrum. However, for processes initiated by strong-field ionization, these wings have a negligible effect. For more demanding applications, the wings can be suppressed by extension of the coherent wavelength multiplexing scheme to include a third OPCPA, centered at 1.5 μm, to fill the spectral gap. The synthesized waveforms are important for optimizing the HHG process, which is to date the only demonstrated technique for generating isolated attosecond pulses [9].

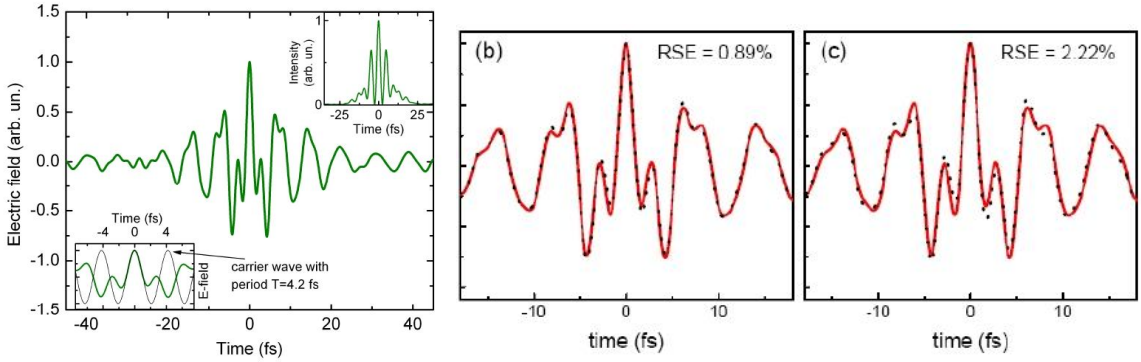

Figure 10: (a) Electric-field waveform of the synthesized sub-cycle pulses, calculated assuming CEPs and a relative timing of φ_1=650 mrad, φ_2=-750 mrad, Δt=0.0 fs optimal for achieving the shortest high-field transient. Lower inset: the waveform is superimposed with the electric field oscillating at the carrier frequency: the synthesized electric-field waveform lasts less than an optical cycle. Upper inset: corresponding intensity profile. (b, c) Waveforms under r.m.s. residual jitters. While the red solid line is the unperturbed waveform of panel (a), the black dotted line is obtained by adding 127 mrad to φ_2 in (b), and 250 as to Δt in (c).

As an example, we numerically solve the time-dependent Schrödinger equation (TDSE) for a He-atom in a strong laser field to illustrate a possible use of our source for driving direct isolated soft-x-ray pulse generation. The achievable peak intensity (6×10^{14} W/cm^2) is chosen such that the total ionization is below the critical ionization level in helium. With choice of CEPs and timing as in Fig. 10(a), substantial ionization is limited to one optical half-cycle and an isolated soft-x-ray pulse spanning over 250 eV is generated without the need for gating techniques [11] or spectral filtering which typically limit the obtainable bandwidth. Using an additional Sn filter, which blocks the strong IR driving field and the nonlinearly chirped low-photon-energy spectral content below 70 eV, leads to an isolated 150-as pulse centered at 200 eV. Of note, the non-sinusoidal electric-field waveform leads to drastically changed electron trajectories (compared to those from a sinusoidal driving field)

resulting in corresponding changes in quantum diffusion and atto-chirp, which can be controlled by means of the waveform synthesis parameters (φ_1, φ_2, and Δt). In this example, quantum diffusion dominates over ionization rate and effectively eliminates the radiation from long trajectories, resulting in isolated soft-x-ray pulse generation solely from short trajectories. This gives an example of the capability of our sub-cycle waveform to simultaneously isolate the ionization process and manipulate electron trajectories within an optical cycle, allowing unprecedented control of the HHG process.

Conclusions

In the fourth and final reporting period of this project we have concluded the theoretical studies on the effects of quantum noise on OPCPAs, and optimized two experimental set-ups for coherent pulse synthesis and CEP-stable single-cycle pulse generation, developed in Milano and at MIT respectively.

In Task 1 we have analyzed noise evolution in OPCPAs, obtaining useful guidelines for their design which is a preliminary step to the pulse synthesis. We have performed a quantum-mechanically consistent numerical investigation of the dynamics of superfluorescence growth in a realistic high-gain OPCPA. Thanks to the model's capability to simulate also the saturation stage of amplification, this investigation for the first time captured all dynamics of a quantum-noise-contaminated OPCPA, addressing the important practical issues of signal energy stability and pulse contrast. These quantities display different evolution dynamics throughout the amplification process. Three operating conditions were explored, characterized by different chirps of the input seed. We find that the chirp maximizing the efficiency-bandwidth product is also characterized by the smallest contribution of the noise. Significantly, we find that while amplifier saturation improves the signal's shot-to-shot energy stability, it does not necessarily improve the pulse contrast. Knowledge of these dynamics increases our fundamental understanding of quantum noise in parametric amplification; it also provides important insight for the optimization of OPCPA systems applied to the study of strong-field laser physics. These results have been published in the following paper:

Cristian Manzoni, Jeffrey Moses, Franz X. Kärtner, and Giulio Cerullo, "Excess quantum noise in optical parametric chirped-pulse amplification," Opt. Express ***19****, 8357-8366 (2011)*

The full text is provided in the Appendix.

In addition a paper has been presented at the Conference on Lasers and Electro-Optics (CLEO) (Munich, Germany, May 22-26 2011) with the title

J. Moses, C. Manzoni, G. Cerullo, and F.X. Kärtner, "Superfluorescence Dynamics of OPCPAs in the Saturation Regime"

The abstract is provided in the Appendix.

In Task 2 we have implemented two different experimental schemes for coherent pulse synthesis. The results can be summarized as follows:

Synthesis from two-stage optical parametric amplification

We have realized a two-stage IR-OPA for the generation of a gap-free phase-stable

ultrabroadband WLC. This setup removes the spectral gap at 800 nm typically arising when spectral broadening the fundamental frequency of a Ti:sapphire laser. The WLC is split in two and used to seed simultaneously the visible NOPA and the degenerate OPA, which are then separately compressed using chirped mirrors to nearly TL duration. The two pulses are combined using a broadband beam splitter and we plan to lock their relative CEP and delay using a nonlinear cross-correlator. Preliminary results demonstrated that combination of the OPA pulses allows obtaining a broadband pulse extending from 550 to 1000 nm, corresponding to a transform-limited duration of 4 fs. Spectral interferometry demonstrated that the delay of the two pulses exhibits fluctuations which can be compensated by a nonlinear correlator. The results of these preliminary experiments have been submitted as a contribution to the "Ultrafast Optics 2011" conference (September 26-30, 2011, Monterey, CA) with the title:

C. Manzoni, S.W. Huang, G. Cirmi, J. Moses, F. X. Kärtner, and G. Cerullo, "Ultrabroadband pulse generation by coherent synthesis of two optical parametric amplifiers"

The abstract of the contribution is given in the appendix.

Sub-cycle pulse synthesis from two OPCPAs

We have developed a scalable optical waveform synthesyzer scheme based on fully controlled coherent wavelength multiplexing of high-energy, few-cycle optical pulses from multi-color OPCPAs. Currently, the system generates a sub-cycle waveform with a spectrum spanning close to two octaves and 15-μJ pulse energy. It can be readily scaled both in energy and bandwidth given the proven wavelength tunability of OPCPAs. A numerical study shows the uniqueness of our source for direct isolated soft-x-ray pulse generation based on HHG, eliminating the need for gating techniques or spectral filtering. The system is capable of stabilizing and controlling all independent parameters that define the synthesized electric-field waveform; this new high-intensity laser architecture can be applied to optical field-emission, tunneling ionization studies, time-resolved spectroscopy, and in general, attosecond control of strong-field physics experiments. The results of this work have been published in the following paper:

S.-W. Huang, G. Cirmi, J. Moses, K.-H. Hong, S. Bhardwaj, J. R. Birge, L.-J. Chen, E. Li, B. J. Eggleton, G. Cerullo, and F. X. Kärtner, "Scalable High-Energy Sub-Cycle Waveform Synthesis for Strong-Field Physics", accepted for publication in ***Nature Photonics*** and currently available on-line. The full text is provided in the Appendix.

References

1. G. Cerullo and S. De Silvestri, “Ultrafast optical parametric amplifiers,” Rev. Sci. Instr. **74**, 1 (2003).
2. T. Wilhelm, J. Piel, and E. Riedle, “Sub-20-fs pulses tunable across the visible from a blue-pumped single-pass noncollinear parametric converter,” Opt. Lett. **22**, 1494-1496 (1997).
3. G. Cerullo, M. Nisoli, and S. De Silvestri, “Generation of 11 fs pulses tunable across the visible by optical parametric amplification”, Appl. Phys. Lett. **71**, 3616-3618 (1997).
4. A. Shirakawa, I. Sakane, and T. Kobayashi, “Pulse-front-matched optical parametric amplification for sub-10-fs pulse generation tunable in the visible and near infrared,” Opt. Lett. **23**, 1292-1294 (1998).
5. G. Cirmi, D. Brida, C. Manzoni, M. Marangoni, S. De Silvestri, and G. Cerullo, “Few-optical-cycle pulses in the near-infrared from a noncollinear optical parametric amplifier,” Opt. Lett. **32**, 2396-2398 (2007).
6. D. Brida, S. Bonora, C. Manzoni, M. Marangoni, P. Villoresi, S. De Silvestri, and G. Cerullo, "Generation of 8.5-fs pulses at 1.3 m for ultrabroadband pump-probe spectroscopy," Opt. Express **17**, 12510-12515 (2009)
7. D. Brida, G. Cirmi, C. Manzoni, S. Bonora, P. Villoresi, S. De Silvestri and G. Cerullo, “Sub-two-cycle light pulses at 1.6 μm from an optical parametric amplifier,” Opt. Lett. **33**, 741-743 (2008).
8. A.L. Cavalieri, E. Goulielmakis, B. Horvarth, W. Helml, M. Schultze, M. Fiess, V. Pervak, L. Veisz, V. Yakovlev, M. Uiberacker, A. Apolonski, F. Krausz, and R. Kienberger, "Intense 1.5-cycle near infrared laser waveforms and their use for the generation of ultra-broadband soft-x-ray harmonic continua," New J. Phys. **9**, 242 (2007).
9. E. Goulielmakis, M. Schultze, M. Hofstetter, V. S. Yakovlev, J. Gagnon, M. Uiberacker, A. L. Aquila, E. M. Gullikson, D. T. Attwood, R. Kienberger, F. Krausz, and U. Kleineberg, "Single-Cycle Nonlinear Optics," Science **320**, 1614-1617 (2008).
10. S. E. Harris, M. K. Oshman, and R. L. Byer, “Observation of Tunable Optical Parametric Fluorescence,” Phys. Rev. Lett. **18**, 732-734 (1967).
11. G. Sansone *et al.*, "Isolated Single-Cycle Attosecond Pulses,". Science **314**, 443-446 (2006).
12. C. W. Gardner, Quantum Noise (Springer-Verlag, Berlin Heidelberg, 1991).
13. A. Gatti, H. Wiedemann, L. A. Lugiato, I. Marzoli, G.-L. Oppo and S. M. Barnett, “Langevin treatment of quantum fluctuations and optical patterns in optical parametric oscillators below threshold,” Phys. Rev. A **56**, 877-897 (1997).
14. J. Chwedenczuk and W. Wasilewski, “Intensity of parametric fluorescence pumped by ultrashort pulses,” Phys. Rev. A **78**, 063823 (2008).
15. R. Graham, “Quantum Statistics in Optics” in Solid State Physics Vol. 66 (Springer-Verlag, Berlin, 1973), pp. 79-81.
16. F. X. Kärtner, R. Schack, and A. Schenzle, “Consistent linearization for quasiprobabilities,” J. Modern Optics **39**, 917-925 (1992).
17. F. X. Kärtner and P. Russer, “Generation of squeezed microwave states by a dc-pumped degenerate parametric Josephson junction oscillator,” Phys. Rev. A **42**, 5601-5612 (1990).
18. F. X. Kärtner , T. Langer, Ch. Ginzel, and A. Schenzle, “Input-output analysis of nonlinear quantum systems in Fokker-Planck approximation,” Phys. Rev. A **45**, 3228-3241, (1992).
19. P. D. Drummond, “Quantum optical tunneling - a representation-free theory valid near the state-equation turning points,” Phys. Rev. A **33**, 4462-4464 (1986).

20. P. Kinsler, “Testing quantum mechanics using third-order correlations,” Phys. Rev. A **53**, 2000 (1996).

21. G. Cerullo, M. Nisoli, S. Stagira, and S. De Silvestri, Opt. Lett **23**, 1283-1285 (1998).

22. A.M. Siddiqui, G. Cirmi, D. Brida, F. X. Kärtner, and G. Cerullo, “Generation of <7 fs pulses at 800 nm from a blue-pumped optical parametric amplifier at degeneracy,” Opt. Lett. **34**, 3592-3594 (2009).

23. A. Baltuška, T. Fuji, and T. Kobayashi, Phys. Rev. Lett. **88**, 133901 (2002).

24. C. Manzoni, D. Polli, G. Cirmi, D. Brida, S. De Silvestri and G. Cerullo, “Tunable few-optical-cycle pulses with passive carrier-envelope phase stabilization from an optical parametric amplifier”, Appl. Phys. Lett. **90**, 171111 (2007).

25. J. Moses, S.-W. Huang, K.-H. Hong, O. D. Mücke, E. L. Falcão-Filho, A. Benedick, F. Ö. Ilday, A. Dergachev, J. A. Bolger, B. J. Eggleton, and F. X. Kärtner, “Highly stable ultrabroadband mid-IR optical parametric chirped-pulse amplifier optimized for superfluorescence suppression,” Opt. Lett. **34**, 1639-1641 (2009).

26. J. Moses, C. Manzoni, S.W. Huang, G. Cerullo, and F.X. Kärtner, “Temporal optimization of ultrabroadband high-energy OPCPA,”. Opt. Express **17**, 5540-5555 (2009).

27. T.R. Schibli *et al.*, “Attosecond active synchronization of passively mode-locked lasers by balanced cross correlation”, Opt. Lett. **28**, 947-949 (2003).

28. J.R. Birge, H.M. Crespo, and F.X. Kärtner, “Theory and design of two-dimensional spectral shearing interferometry for few-cycle pulse measurement”, J. Opt. Soc. Am. B **27**, 1165-1173 (2010).

29. X. Gu, G. Marcus, Y. Deng, T. Metzger, C. Teisset, N. Ishii, T. Fuji, A. Baltuska, R. Butkus, V. Pervak, H. Ishizuki, T. Taira, T. Kobayashi, R. Kienberger, and F. Krausz, “Generation of carrier-envelope-phase-stable 2-cycle 740- J pulses at 2.1- m carrier wavelength,” Opt. Express **17**, 62-69 (2009).

30. F. Haake, H. King, G. Schröder, J. Haus, R. Glauber, F. Hopf, “Macroscopic Quantum Fluctuations in Superfluorescence,” Phys. Rev. Lett. 42, 1740-1743 (1979).

31. S.-W. Huang, G. Cirmi, J. Moses, K.-H. Hong, S. Bhardwaj1, J. R. Birge, L.-J. Chen, E. Li, B. J. Eggleton, G. Cerullo, and F. X. Kärtner, “Scalable High-Energy Sub-Cycle Waveform Synthesis for Strong-Field Physics”, accepted for publication in Nature Photonics

List of Symbols, Abbreviations, and Acronyms

2DSI: two-dimensional spectral-shearing interferometer
AOPDF: Acousto-Optic Programmable Dispersive Filter
BBO: β-Barium Borate
BCC Balanced cross-correlator
CEP: Carrier-Envelope Phase
CPA: Chirped Pulse Amplification
DCM: double-chirped mirror
DFG: Difference Frequency Generation
FF: Fundamental Frequency
FWHM: Full Width at Half Maximum
HHG: High-Harmonic Generation
IR: Infrared
NIR-OPCPA: near infrared OPCPA
NOPA: Noncollinear Optical Parametric Amplifier
OPA: Optical Parametric Amplifier
OPCPA: Optical Parametric Chirped Pulse Amplification
OR: Optical Rectification
PPLN: Periodically-Poled Lithium Niobate
PSF: parametric superfluorescence
SH: Second Harmonic
SNR: Signal-to-Noise Ratio
SPR: Signal-to-Pedestal Ratio
SWIR-OPCPA: short-wavelength infrared OPCPA
TDSE: time-dependent Schrödinger equation
TL: Transform Limit
WD: Wigner distribution
WLC: white light continuum
YDFA: Ytterbium-doped fiber amplifier

List of publications from the project

The results obtained in the framework of the whole project are of great scientific relevance, and have been published as journal articles and contributions to international conferences. In the following we include a list of papers and conferences contributions:

Journal articles:

S.-W. Huang, G. Cirmi, J. Moses, K.-H. Hong, S. Bhardwaj, J. R. Birge, L.-J. Chen, E. Li, B. J. Eggleton, G. Cerullo, and F. X. Kärtner, "Scalable High-Energy Sub-Cycle Waveform Synthesis for Strong-Field Physics", accepted for publication in ***Nature Photonics*** *and currently available on-line.*

C. Manzoni, J. Moses, F. X. Kärtner, and G. Cerullo, "Excess quantum noise in optical parametric chirped-pulse amplification," Opt. Express ***19****, 8357-8366 (2011)*

F. Junginger, A. Sell, O. Schubert, B. Mayer, D. Brida, M. Marangoni, G. Cerullo, A. Leitenstorfer, and R. Huber, "Single-cycle multiterahertz transients with peak fields above 10 MV/cm," Opt. Lett. ***35****, 2645-2647 (2010)*

A. M. Siddiqui, G. Cirmi, D. Brida, F. X. Kärtner, and G. Cerullo, "Generation of <7 fs pulses at 800 nm from a blue-pumped optical parametric amplifier at degeneracy," Opt. Lett. ***34****, 3592-3594 (2009).*

J. Moses, C. Manzoni, S.-W. Huang, Giulio Cerullo, and Franz X. Kartner, "Temporal Optimization of Ultrabroadband High-Energy OPCPA", Optics Express ***17****, 5540-5555 (2009)*

Contributions to conferences:

- Ultrafast Optics 2011 (Monterey, CA, September 26-30, 2011):
C. Manzoni, S.W. Huang, G. Cirmi, J. Moses, F. X. Kärtner, and G. Cerullo, "Ultrabroadband pulse generation by coherent synthesis of two optical parametric amplifiers"

- Conference on Lasers and Electro-Optics (CLEO) (Munich, Germany, May 22-26 2011):
J. Moses, C. Manzoni, G. Cerullo, and F.X. Kärtner, "Superfluorescence Dynamics of OPCPAs in the Saturation Regime"

- Conference on Laser and Electro Optics (San Jose, California, USA, May 16-21, 2010):
Shu-Wei Huang, Giovanni Cirmi, Jeffrey Moses, Kyung-Han Hong, Andrew Benedick, Li-Jin Chen, Enbang Li, Benjamin Eggleton, Giulio Cerullo and Franz X. Kärtner, "Ultrabroadband Optical Parametric Chirped Pulse Amplifier System for Single-Cycle Waveform Synthesis".

- 17th International Conference on Ultrafast Phenomena (Snowmass Village, Colorado, USA, July 18–23, 2010):
C. Manzoni, J. Moses, F. X. Kärtner, and G. Cerullo, "The Evolution of Signal-to-noise Ratio in Superfluorescence-contaminated Optical Parametric Chirped-pulse Amplification"

- Conference on Lasers and Electro-Optics (CLEO) (Baltimore, Maryland, USA, May 31 – June 5 2009):
J. Moses, C. Manzoni, S.-W. Huang, G. Cerullo, F.X. Kärtner, "Multi-Stage Optimization of Ultrabroadband High-Energy Optical Parametric Chirped Pulse Amplification"

Appendix – Papers and conference contributions

We append to this document the papers and conference submissions related to the activity of the fourth reporting period.

Journal articles:

S.-W. Huang, G. Cirmi, J. Moses, K.-H. Hong, S. Bhardwaj, J. R. Birge, L.-J. Chen, E. Li, B. J. Eggleton, G. Cerullo, and F. X. Kärtner, "Scalable High-Energy Sub-Cycle Waveform Synthesis for Strong-Field Physics", accepted for publication in ***Nature Photonics*** *and currently available on-line*

C. Manzoni, J. Moses, F. X. Kärtner, and G. Cerullo, "Excess quantum noise in optical parametric chirped-pulse amplification," Opt. Express ***19****, 8357-8366 (2011)*

Contributions to conferences:

"Ultrafast Optics 2011" conference (September 26-30, 2011, Monterey, CA):
C. Manzoni, S.W. Huang, G. Cirmi, J. Moses, F. X. Kärtner, and G. Cerullo, "Ultrabroadband pulse generation by coherent synthesis of two optical parametric amplifiers"

Conference on Lasers and Electro-Optics (CLEO) (Munich, Germany, May 22-26 2011) with the title:
J. Moses, C. Manzoni, G. Cerullo, and F.X. Kärtner, "Superfluorescence Dynamics of OPCPAs in the Saturation Regime"

nature photonics

LETTERS

PUBLISHED ONLINE: 24 JULY 2011 | DOI: 10.1038/NPHOTON.2011.140

High-energy pulse synthesis with sub-cycle waveform control for strong-field physics

Shu-Wei Huang[1], Giovanni Cirmi[1], Jeffrey Moses[1], Kyung-Han Hong[1], Siddharth Bhardwaj[1], Jonathan R. Birge[1], Li-Jin Chen[1], Enbang Li[2], Benjamin J. Eggleton[2], Giulio Cerullo[3] and Franz X. Kärtner[1,4]*

Over the last decade, control of atomic-scale electronic motion by non-perturbative optical fields has broken tremendous new ground with the advent of phase-controlled high-energy few-cycle pulse sources[1]. The development of close to single-cycle, carrier-envelope phase controlled, high-energy optical pulses has already led to isolated attosecond EUV pulse generation[2], expanding ultrafast spectroscopy to attosecond resolution[1]. However, further investigation and control of these physical processes requires sub-cycle waveform shaping, which has not been achievable to date. Here, we present a light source, using coherent wavelength multiplexing, that enables sub-cycle waveform shaping with a two-octave-spanning spectrum and a pulse energy of 15 μJ. It offers full phase control and allows generation of any optical waveform supported by the amplified spectrum. Both energy and bandwidth scale linearly with the number of sub-modules, so the peak power scales quadratically. The demonstrated system is the prototype of a class of novel optical tools for attosecond control of strong-field physics experiments.

Since the invention of pulsed lasers, the ultrafast laser science community has strived for ever broader optical bandwidths, shorter pulse durations, higher pulse energies and improved phase control. Each breakthrough in generation methods has led to new scientific discoveries in a wide range of fields[3–5]. Recent investigations of phenomena at the intersection of ultrafast and strong-field laser physics, such as high-harmonic generation (HHG)[6] and strong-field ionization[7], have demanded that laser sources combine each of the breakthroughs mentioned above. Investigation and control of the strong-field light–matter interaction simultaneously requires a multi-octave-spanning bandwidth, an isolated sub-cycle waveform, peak intensity above 1×10^{14} W cm^{-2} and full phase control. Such features would allow arbitrary shaping of the strong electric-field waveform for steering ionized electron wave packets[8] and precise control of tunnelling and multi-photon ionization events.

For over two decades, laser scientists have sought to extend laser bandwidths and achieve sub-cycle optical waveforms by synthesizing multiple laser sources[9]. Attempts to combine two independent mode-locked lasers have met with some success, for example in frequency metrology[10,11], but are challenging because of the differential phase noise beyond the achievable feedback loop bandwidth. This problem was recently circumvented by coherently adding two pulse trains derived from the same fibre laser, resulting in the first demonstration of an isolated single-cycle optical pulse source[12]. This proved the feasibility of pulse synthesis at the nanojoule level, but achieving high pulse energy requires the synthesis of low-repetition-rate pulses, which is a challenge because of the environmental perturbations typical of high-energy amplifiers. An approach to high-energy pulse synthesis based on combining the pump, signal and idler of a multi-cycle optical parametric amplifier is being investigated, and shows the potential to produce multiple single-cycle pulses under a multi-cycle envelope with pulse separation on the order of a few femtoseconds[13].

In this Letter, we address the challenge of high-energy sub-cycle optical waveform synthesis. We demonstrate a new approach, based on coherent wavelength multiplexing of ultra-broadband optical parametric chirped pulse amplifiers (OPCPAs), for the generation of fully controlled high-energy non-sinusoidal optical waveforms with spectra spanning close to two octaves. By means of simulation, we present an example of the unique features of our source as a driver for isolated strong-field physics experiments: the confinement of the strong-field light–matter interaction to within an optical cycle and attosecond control of the interaction. The system coherently combines two carrier-envelope phase (CEP)-controlled, few-cycle pulses obtained from different OPCPAs: (i) a near-infrared (NIR) OPCPA, producing 25 μJ, 9 fs pulses centred at 870 nm and (ii) a short-wavelength infrared (SWIR) OPCPA, producing 25 μJ, 24 fs pulses centred at 2.15 μm. The ultra-broadband OPCPA is the most promising technology for producing wavelength-tunable, high-peak-power and high-average-power, few-cycle optical pulses with good pre-pulse contrast[14]. Furthermore, an ultra-broadband OPCPA maintains good CEP stability due to the low thermal load and the small dispersion required to stretch and compress the signals.

Figure 1 shows a schematic of the system. It starts with an actively CEP-stabilized octave-spanning Ti:sapphire oscillator. Using a single oscillator as the front-end for the entire system ensures the coherence of the two OPCPA pulses to within environmental fluctuations and drifts on subsequent beam paths. The designs of the OPCPAs follow the guidelines described in previous studies[15,16] for simultaneously optimizing energy conversion, amplification bandwidth and signal-to-noise ratio. Of note, the inclusion of an acousto-optic programmable dispersive filter (AOPDF) in each OPCPA allows independent spectral phase and amplitude adjustment of each pulse, enabling control and optimization of the synthesized waveform.

Outputs from the two OPCPAs are combined in a broadband neutral beamsplitter. The overall spectrum spans over 1.8 octaves (green lines in Fig. 2a), and the energy of the synthesized pulse is 15 μJ. Besides the spectral phases (controlled by the AOPDFs),

[1]Department of Electrical Engineering and Computer Science and Research Laboratory of Electronics, Massachusetts Institute of Technology, Cambridge, Massachusetts 02139, USA, [2]Centre for Ultrahigh Bandwidth Devices for Optical Systems, Australian Research Council Centre of Excellence, School of Physics, University of Sydney, NSW 2006, Australia, [3]IFN-CNR, Dipartimento di Fisica, Politecnico di Milano, Piazza L. Da Vinci 32, 20133 Milano, Italy, [4]DESY-Center for Free-Electron Laser Science and Hamburg University, Notkestraße 85, D-22607 Hamburg, Germany. *e-mail: kaertner@mit.edu

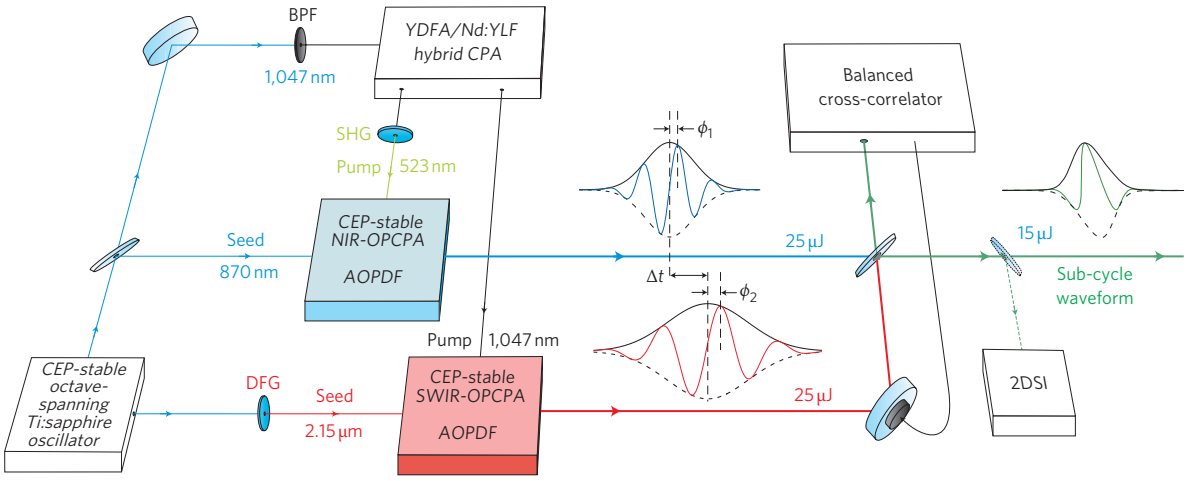

Figure 1 | Schematic of the high-energy optical waveform synthesizer. Two CEP-stabilized, few-cycle OPCPAs centred at different wavelengths are combined based on the concept of coherent wavelength multiplexing to produce a fully controlled non-sinusoidal optical waveform with a pulse energy of 15 μJ at a repetition rate of 1 kHz. Full control over the optical phase allows for any optical waveform given the amplified spectrum. YDFA, ytterbium-doped fibre amplifier; BPF, bandpass filter; DFG, difference frequency generation (intra-pulse).

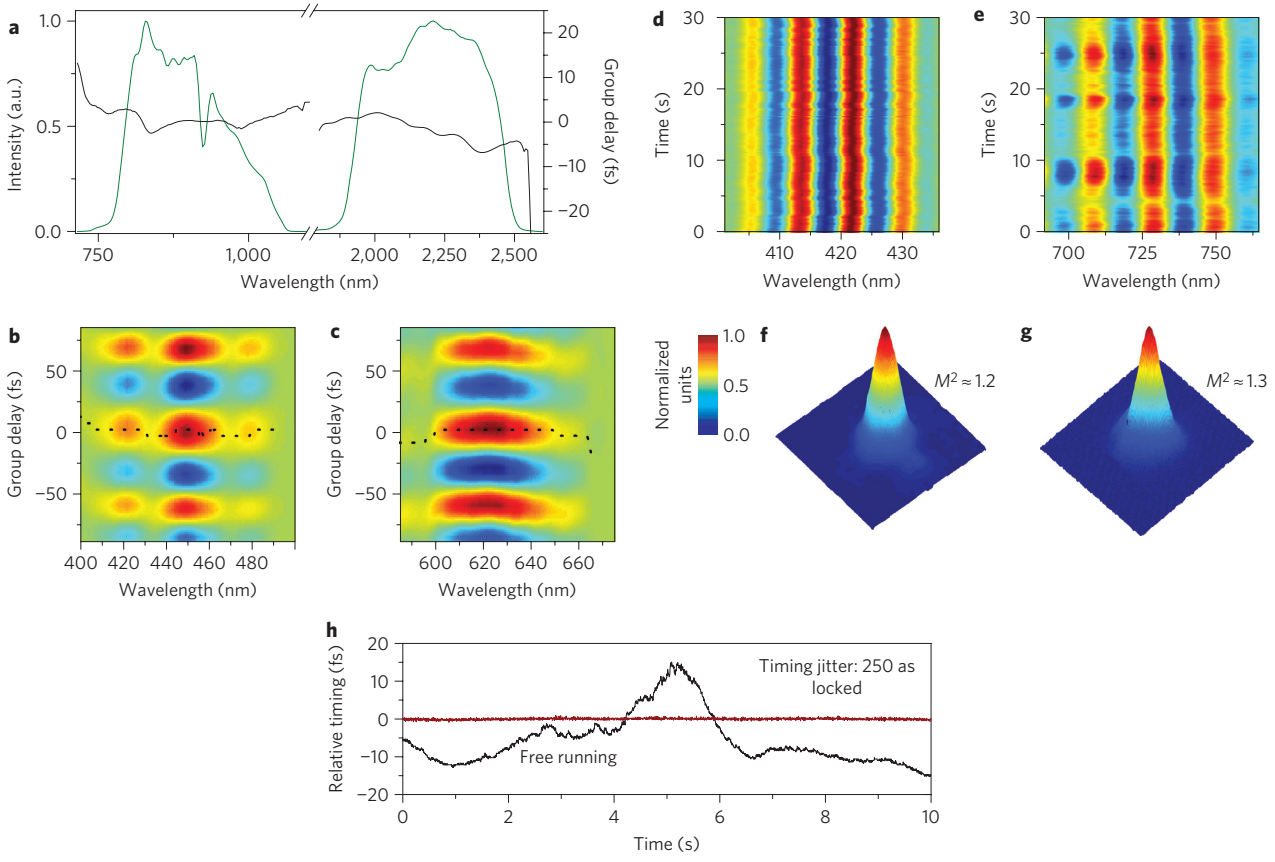

Figure 2 | Characterization of the synthesized pulses. a, Optical spectrum (green) and frequency-dependent group delay (black) of the synthesized pulses. The overall spectrum spans over 1.8 octaves and supports non-sinusoidal waveforms with sub-cycle features. **b**,**c**, 2DSI trace for the NIR OPCPA (**b**) and the SWIR OPCPA (**c**). The 2DSI measurements show that the two pulses are temporally overlapped and well compressed to within 10% of the transform-limited pulse duration. CEP stabilities are verified using nonlinear interferograms with five-shot integration. **d**, *f*–2*f* interferogram, measuring 135 mrad r.m.s. CEP fluctuations over 30 s for the NIR OPCPA. **e**, *f*–3*f* interferogram, measuring 127 mrad r.m.s. CEP fluctuations over 30 s for the SWIR OPCPA. Spatial properties are characterized by measuring the beam profiles and the M^2 values. **f**,**g**, Beam profile of the NIR OPCPA (**f**) and the SWIR OPCPA (**g**). The M^2 value of the NIR-OPCPA is 1.2 and that of the SWIR OPCPA is 1.3. The BCC-assisted feedback loop guarantees the relative timing stability. **h**, BCC measurements of the free-running (black) and closed-loop (red) systems. The closed-loop system ensures a relative timing drift of 250 as, less than 5% of the oscillation period of the SWIR OPCPA (over 10 s).

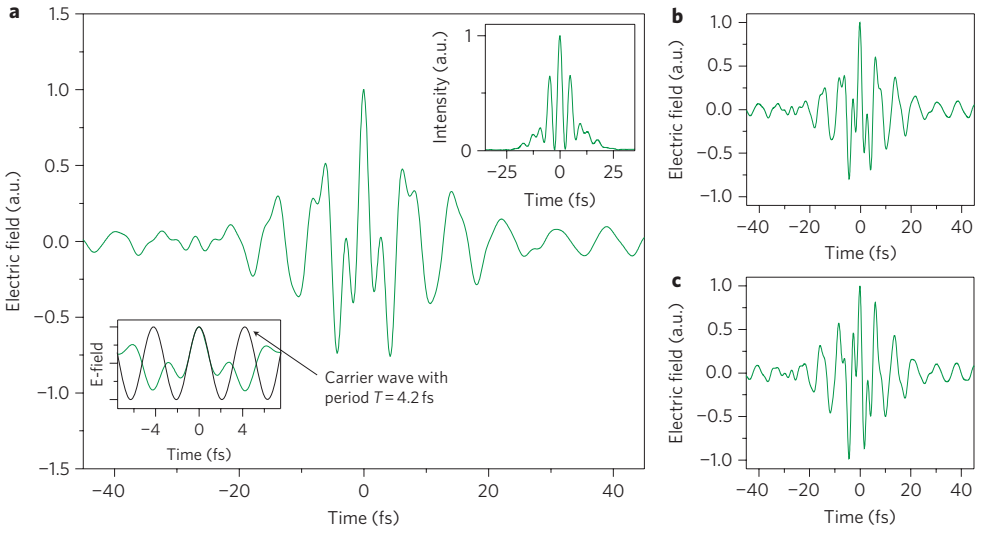

Figure 3 | The synthesized electric-field waveforms. a, Here, we assume CEPs ($\phi_1 = 650$ mrad, $\phi_2 = -750$ mrad) optimal for achieving the shortest high-field transient, which lasts only 0.8 cycles (amplitude FWHM) of the carrier (centroid) frequency. Lower inset: the waveform is plotted in a shorter time window and superimposed with an electric field oscillating at the carrier (centroid) frequency, showing that the synthesized electric-field waveform is non-sinusoidal and the main feature lasts less than an optical cycle. Upper inset: corresponding intensity profile. About one-third of the pulse energy is contained in the main pulse. As an example of waveform shaping made possible by tuning the parameters of our system, two additional atypical waveforms are shown. **b**, A waveform synthesized by adding 500 mrad to both ϕ_1 and ϕ_2. **c**, A waveform synthesized by adding 1 fs to Δt.

three other independent parameters (Fig. 1) determine the synthesized electric-field waveform: the CEP of the NIR OPCPA pulse (ϕ_1), the CEP of the SWIR OPCPA pulse (ϕ_2) and the relative timing between the two OPCPA pulses (Δt). Precise stabilization of these three parameters is required for coherent synthesis of the two OPCPA pulses, and subsequent control of each parameter allows precise waveform shaping. Although the CEP of the SWIR OPCPA is passively stabilized due to the intrapulse difference-frequency generation (DFG)[17] used to produce its seed, an active feedback loop on the oscillator is implemented to ensure the CEP stability of the NIR OPCPA. Figure 2d,e demonstrates the CEP stability of the two individual pulses, with r.m.s. fluctuations as low as 135 mrad and 127 mrad, respectively. Figure 2h characterizes the relative timing stability. A feedback loop based on a balanced cross-correlator (BCC)[18] is implemented to synchronize the two pulses, allowing attosecond-precision relative timing stability. With the feedback control of the SWIR OPCPA's path length over a bandwidth of 30 Hz, the relative timing drift is reduced to 250 as, less than 5% of the oscillation period of the SWIR OPCPA (7.2 fs).

Once the BCC-assisted feedback loop stabilizes the relative timing between the two OPCPA pulses, a two-dimensional spectral-shearing interferometer (2DSI)[19] is used to measure the frequency-dependent group delay of the synthesized pulse. Figure 2b,c presents the raw data of a 2DSI measurement, and Fig. 2a plots (black lines) the extracted frequency-dependent group delay of the synthesized pulse, which is the derivative of the spectral phase with respect to frequency. The 2DSI measurement shows that the two OPCPA pulses are temporally overlapped, and each is well compressed to within 10% of its transform-limited pulse duration.

In our system, the CEPs can be varied by slight tuning of any dispersive element, including the AOPDFs[20]. The values of the CEP will be determined automatically *in situ* when strong-field experiments are conducted[21], so CEP tunability is sufficient from an experimental point of view. In summary, our system is capable of stabilizing and controlling all independent parameters that define the synthesized electric-field waveform. Figure 3a plots a synthesized electric-field waveform and intensity profile assuming the CEPs ($\phi_1 = 650$ mrad, $\phi_2 = -750$ mrad) optimal for achieving the shortest high-field transient, which lasts only 0.8 cycles (amplitude FWHM) of the carrier (centroid) frequency ($\lambda_c = 1.26$ μm). The lower inset of Fig. 3a clearly shows that the synthesized electric-field waveform is non-sinusoidal, and the main feature lasts less than an optical cycle. As an example of waveform shaping made possible by tuning the parameters of our system, Fig. 3b,c shows two atypical waveforms as the CEP and relative timing are changed. Because of the large gap in the combined spectrum, there are wings 4.8 fs from the central peak, as shown in Fig. 3a. As we will show below, for processes initiated by strong-field ionization, these wings have a negligible effect. For more demanding applications, the wings can be suppressed by extension of the coherent wavelength multiplexing scheme to include a third OPCPA, centred at 1.5 μm (ref. 22), to fill the spectral gap. The synthesized waveforms are important for optimizing the HHG process[6], which is, to date, the only demonstrated technique for generating isolated attosecond pulses[2]. As an example, we numerically solve the time-dependent Schrödinger equation (TDSE) for a helium atom in a strong laser field to illustrate a possible use of our source for driving direct isolated soft X-ray pulse generation (Fig. 4). The achievable peak intensity (6×10^{14} W cm^{-2}) is chosen such that the total ionization is below the critical ionization level in helium[23]. With the choice of CEPs as in Fig. 4a, substantial ionization is limited to one optical half-cycle, and an isolated soft X-ray pulse spanning over 250 eV is generated (Fig. 4b,c) without the need for gating techniques[24] or spectral filtering, which typically limit the obtainable bandwidth. Using an additional tin filter, which blocks the strong IR driving field and the nonlinearly chirped low-photon-energy spectral content below 70 eV, leads to an isolated 150 as pulse centred at 200 eV. Of note, the non-sinusoidal electric-field waveform leads to drastically changed electron trajectories (compared to those from a sinusoidal driving field), resulting in corresponding changes in quantum diffusion and atto-chirp, which can be controlled by means of the waveform synthesis parameters (ϕ_1, ϕ_2 and Δt). In this example, quantum diffusion dominates over ionization rate (see Supplementary Information) and effectively eliminates the radiation from long trajectories, resulting in isolated soft X-ray pulse generation solely from short trajectories (Fig. 4b). This gives an example of the capability of our light source

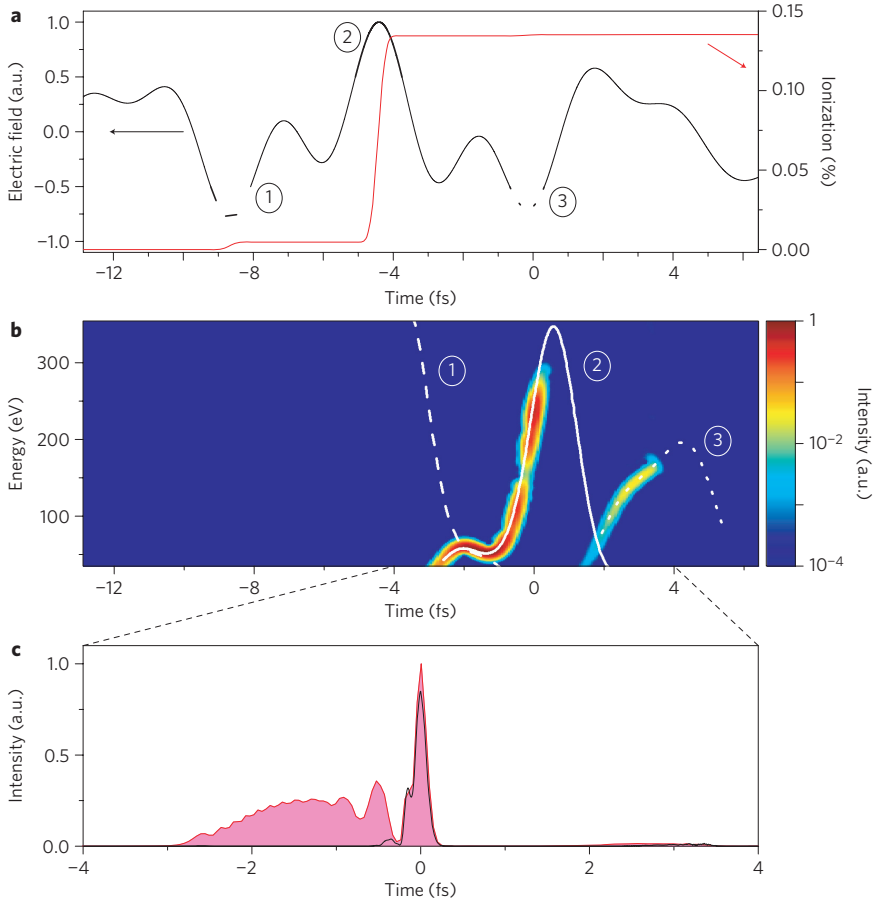

Figure 4 | Extreme nonlinear optics with sub-cycle manipulated waveforms. TDSE simulation results of the single-atom HHG show the uniqueness of our source for direct isolated soft X-ray pulse generation. **a**, Ionization dynamics (red) induced in helium by a linearly polarized electric-field waveform (black) assuming a peak intensity of 6×10^{14} W cm^{-2}, $\phi_1 = 960$ mrad and $\phi_2 = -440$ mrad. **b**, Spectrogram of the HHG superimposed with the calculated classical trajectories. Returning trajectories from three ionization events (2, main pulse; 1 and 3, satellite pulses) are shown for clear interpretation of the spectrogram. The synthesized pulse isolates the ionization process to a half optical cycle, and a continuum spectrum spanning more than 250 eV can be achieved. The isolated soft X-ray pulse has the same sign of chirp over 80% of the spectrum, so the compression setup can be simplified. **c**, Isolated soft X-ray pulse plotted in the time domain before (pink) and after (black line) a 100-nm-thick Sn filter. The Sn filter is chosen for its ability to block the strong IR driving field and the nonlinearly chirped low-photon-energy spectral content, and its good transmission in the soft X-ray range. The filtered isolated soft X-ray pulse has a FWHM duration of 150 as.

to simultaneously isolate the ionization process and manipulate electron trajectories within an optical cycle, allowing unprecedented control of the HHG process.

In conclusion, we have presented a scalable waveform synthesis scheme based on fully controlled coherent wavelength multiplexing of high-energy, few-cycle optical pulses from multi-colour OPCPAs. Currently, the system generates a non-sinusoidal waveform that can be used to drive isolated strong-field physics experiments. The pulse energy is 15 μJ, with the spectrum spanning close to two octaves, and it can be readily scaled both in energy and bandwidth given the proven wavelength tunability of OPCPAs[25] (see Supplementary Information). A numerical study shows the uniqueness of our source for direct isolated soft X-ray pulse generation based on HHG, eliminating the need for gating techniques[24] or spectral filtering. In addition to this application, this new high-intensity laser architecture can be applied to optical field-emission[26], tunnelling ionization studies[27], time-resolved spectroscopy[28] and, in general, attosecond control of strong-field physics experiments.

Methods

OPCPA setup. The system schematic is presented in Supplementary Fig. S1. Both OPCPAs are pumped by an optically synchronized (injection seeded by the Octavius-85M Ti:sapphire oscillator from IdestaQE, Inc.) Nd:YLF chirped pulse amplifier (CPA), which generates 3.5 mJ, 12 ps pulses at 1,047 nm. The SWIR OPCPA, pumped by 1 mJ of the Nd:YLF CPA output, follows the design method in ref. 15. The seed, produced by intrapulse DFG of the oscillator, is first stretched by a bulk silicon block to 5 ps and pre-amplified to 1.5 μJ in the first OPCPA stage using periodically poled lithium niobate (PPLN). The pre-amplified pulse is further stretched to 9.5 ps by an infrared AOPDF, amplified to 25 μJ in periodically poled stoichiometric lithium tantalate (PPSLT), and then compressed to 24 fs in a broadband anti-reflection coated quartz glass block (Suprasil 300). For the NIR OPCPA, a 2 mJ fraction of the Nd:YLF CPA output is frequency-doubled in a lithium triborate (LBO) crystal and used to amplify the oscillator output. The seed is first stretched to 5 ps by a Brewster prism stretcher. The signal is pre-amplified in a double-pass configuration in a type-I, 5-mm-long β-barium borate (BBO) crystal to 2 μJ. The amplified pulse is further stretched to 6.2 ps by an AOPDF and a grating stretcher, amplified to 25 μJ in BBO and then compressed to 9 fs in a Brewster-cut N-LaSF9 block.

Beam combining. The outputs of the two OPCPAs are combined in a broadband neutral beamsplitter, which introduces 25% energy loss. In addition, only half of the synthesized pulse energy is available for experiments, because the other half is directed to the balanced cross-correlator (BCC). Because the pulse energy directed to the BCC is much greater than is needed, a custom-made dichroic mirror can be implemented to improve the experimentally available pulse energy by a factor of 2.5. Thus, in an optimized system, waveform synthesis could be achieved with very low losses.

We chose to combine the two OPCPA pulses in a 'constant waist width' fashion[29], which is inherently compatible with OPCPA configurations. As shown theoretically in ref. 29, the 'constant waist width' configuration offers the unique property that the temporal pulse form remains unchanged upon propagation.

Relative timing stabilization. One part of the combined beam is directed to a BCC (Supplementary Fig. S2), which consists of two nearly identical cross-correlators using 200-μm-thick BBO crystals, phase-matched for sum-frequency generation of 870 nm light and 2.15 μm light. Use of the SWIR OPCPA delay stage and a 4-mm-thick calcium fluoride (CaF_2) window between cross-correlators sets the group delay between pulses to +25 fs in one cross-correlator and −25 fs in the other. An additional 2-mm-thick calcium fluoride window ensures zero group delay ($\Delta t = 0.0$ fs) at the combined output. For deviations from this zero-delay configuration of up to ±20 fs, the photodetector signal is linearly proportional to the time difference and thus can be used as the error signal fed to the loop filter in the feedback system. Furthermore, in the vicinity of the zero crossing, the setup delivers a balanced signal and thus the amplitude noise of each OPCPA output does not affect the detected error signal.

2DSI. In the 2DSI setup (Supplementary Fig. S3), the combined beam is first split by a beam sampler in which the second surface is anti-reflection coated. A copy of the beam (4%) is Fresnel-reflected and only guided via silver mirrors before being mixed in a 40 μm type II BBO. The other copy of the beam (96%) passes through the beam sampler and is highly stretched before being equally split again by a cube beamsplitter, routed to the BBO and mixed with the unchirped pulse. Two collinear, temporally overlapped, but spectrally sheared up-converted pulses are then generated. To observe the interference between the two up-converted pulses, which encodes the spectral group delay information, the delay of one of the highly chirped pulses is scanned over a few optical cycles. The spectrum of the up-converted signal is recorded as a function of this delay, yielding a two-dimensional intensity function that is shown in Fig. 2b,c. The interpretation of the 2DSI data is relatively straightforward; each spectral component is vertically shifted in proportion to its group delay.

It should be noted that we treat the combined beam as a single pulse, and use the 2DSI to retrieve the frequency-dependent group delay of the synthesized pulse, and not just those of the individual OPCPA pulses. That is, we measured the combined beam, not the two OPCPA pulses independently, and the portion mixed with the unchirped pulse is purely derived from the NIR OPCPA such that the measured spectral group delay has a definite reference throughout the whole spectrum from 700 to 2,500 nm. A different relative timing results in a vertical shift of the fringe patterns in Fig. 2b,c.

Received 23 February 2011; accepted 5 June 2011; published online 24 July 2011

References

1. Krausz, F. & Ivanov, M. Attosecond physics. *Rev. Mod. Phys.* **81,** 163–234 (2009).
2. Goulielmakis, E. *et al.* Single-cycle nonlinear optics. *Science* **320,** 1614–1617 (2008).
3. Udem, T., Holzwarth, R. & Hänsch, T. W. Optical frequency metrology. *Nature* **416,** 233–237 (2002).
4. Kienberger, R. *et al.* Atomic transient recorder. *Nature* **427,** 817–821 (2004).
5. Li, C. H. *et al.* A laser frequency comb that enables radial velocity measurements with a precision of 1 cm s^{-1}. *Nature* **452,** 610–612 (2008).
6. Corkum, P. B. Plasma perspective on strong field multiphoton ionization. *Phys. Rev. Lett.* **71,** 1994–1997 (1993).
7. Keldysh, L. V. Ionization in the field of a strong electromagnetic wave. *Sov. Phys. JETP* **20,** 1307–1314 (1965).
8. Chipperfield, L. E., Robinson, J. S., Tisch, J. W. G. & Marangos, J. P. Ideal waveform to generate the maximum possible electron recollision energy for any given oscillation period. *Phys. Rev. Lett.* **102,** 063003 (2009).
9. Hänsch, T. W. A proposed sub-femtosecond pulse synthesizer using separate phase-locked laser oscillators. *Opt. Commun.* **80,** 71–75 (1990).
10. Wei, Z. Y., Kobayashi, Y., Zhang, Z. G. & Torizuka, K. Generation of two-color femtosecond pulses by self-synchronizing Ti:sapphire and Cr:forsterite lasers. *Opt. Lett.* **26,** 1806–1808 (2001).
11. Shelton, R. K. *et al.* Phase-coherent optical pulse synthesis from separate femtosecond lasers. *Science* **293,** 1286–1289 (2001).
12. Krauss, G. *et al.* Synthesis of a single cycle of light with compact erbium-doped fibre technology. *Nature Photon.* **4,** 33–36 (2010).
13. Cerullo, G., Baltuška, A., Mücke, O. D. & Vozzi, C. Few-optical-cycle light pulses with passive carrier-envelope phase stabilization. *Laser Photon. Rev.* **5,** 323–351 (2011).
14. Dubietis, A., Butkus, R. & Piskarskas, A. P. Trends in chirped pulse optical parametric amplification. *IEEE J. Sel. Top. Quantum Electron.* **12,** 163–172 (2006).
15. Moses, J. *et al.* Highly stable ultrabroadband mid-IR optical parametric chirped-pulse amplifier optimized for superfluorescence suppression. *Opt. Lett.* **34,** 1639–1641 (2009).
16. Moses, J., Manzoni, C., Huang, S. W., Cerullo, G. & Kärtner, F. X. Temporal optimization of ultrabroadband high-energy OPCPA. *Opt. Express* **17,** 5540–5555 (2009).
17. Baltuška, A., Fuji, T. & Kobayashi, T. Controlling the carrier-envelope phase of ultrashort light pulses with optical parametric amplifiers. *Phys. Rev. Lett.* **88,** 1339011 (2002).
18. Schibli, T. R. *et al.* Attosecond active synchronization of passively mode-locked lasers by balanced cross correlation. *Opt. Lett.* **28,** 947–949 (2003).
19. Birge, J. R., Crespo, H. M. & Kärtner, F. X. Theory and design of two-dimensional spectral shearing interferometry for few-cycle pulse measurement. *J. Opt. Soc. Am. B* **27,** 1165–1173 (2010).
20. Forget, N., Canova, L., Chen, X., Jullien, A. & Lopez-Martens, R. Closed-loop carrier-envelope phase stabilization with an acousto-optic programmable dispersive filter. *Opt. Lett.* **34,** 3647–3649 (2009).
21. Wittmann, T. *et al.* Single-shot carrier-envelope phase measurement of few-cycle laser pulses. *Nature Phys.* **5,** 357–362 (2009).
22. Mücke, O. D. *et al.* Scalable Yb-MOPA-driven carrier-envelope phase-stable few-cycle parametric amplifier at 1.5 μm. *Opt. Lett.* **34,** 118–120 (2009).
23. Popmintchev, T. *et al.* Phase matching of high harmonic generation in the soft and hard X-ray regions of the spectrum. *Proc. Natl Acad. Sci. USA* **106,** 10516–10521 (2009).
24. Sansone, G. *et al.* Isolated single-cycle attosecond pulses. *Science* **314,** 443–446 (2006).
25. Cerullo, G. & De Silvestri, S. Ultrafast optical parametric amplifiers. *Rev. Sci. Instrum.* **74,** 1–18 (2003).
26. Hommelhoff, P., Kealhofer, C. & Kasevich, M. A. Ultrafast electron pulses from a tungsten tip triggered by low-power femtosecond laser pulses. *Phys. Rev. Lett.* **97,** 247402 (2006).
27. Arissian, L. *et al.* Direct test of laser tunneling with electron momentum imaging. *Phys. Rev. Lett.* **105,** 133002 (2010).
28. Hochstrasser, R. M. Two-dimensional spectroscopy at infrared and optical frequencies. *Proc. Natl Acad. Sci. USA* **104,** 14190–14196 (2007).
29. Zou, Q. H. & Lu, B. Propagation properties of ultrashort pulsed beams with constant waist width in free space. *Opt. Laser Technol.* **39,** 619–625 (2007).

Acknowledgements

This work was supported by the Air Force Office of Scientific Research (grants FA9550-09-1-0212, FA8655-09-1-3101 and FA9550-10-1-0063) and by Progetto Roberto Rocca.

Author contributions

F.X.K., K.H.H., J.M. and S.W.H. conceived the experiment, and carried it out together with G.Ce. and G.Ci.; S.B. provided the TDSE simulation and the spectrogram analysis; J.R.B. provided critical discussion on 2DSI; L.J.C. provided critical help and discussion on the Ti:sapphire oscillator; E.L. and B.J.E. provided the chirped fibre Bragg grating; S.W.H., G.Ci., K.H.H., J.M., F.X.K. and G.Ce. co-wrote the paper. F.X.K. is the senior author of the group and supervised the work.

Additional information

The authors declare no competing financial interests. Supplementary information accompanies this paper at www.nature.com/naturephotonics. Reprints and permission information is available online at http://www.nature.com/reprints/. Correspondence and requests for materials should be addressed to F.X.K.

Excess quantum noise in optical parametric chirped-pulse amplification

Cristian Manzoni,[1,*] Jeffrey Moses,[2] Franz X. Kärtner,[2,3] and Giulio Cerullo[1]

[1]*IFN-CNR, Dipartimento di Fisica, Politecnico di Milano, Piazza L. da Vinci 32, 20133 Milano, Italy*
[2]*Department of Electrical Engineering and Computer Science and Research Laboratory of Electronics, Massachusetts Institute of Technology, Cambridge, Massachusetts 02139, USA*
[3]*DESY - Center for Free-Electron Laser Science and Department of Physics, Hamburg University, D-22607 Hamburg, Germany*
**cristian.manzoni@polimi.it*

Abstract: Noise evolution in an optical parametric chirped-pulse amplifier (OPCPA) differs essentially from that of an optical parametric or a conventional laser amplifier, in that an incoherent pedestal is produced by superfluorescence that can overwhelm the signal under strong saturation. Using a model for the nonlinear dynamics consistent with quantum mechanics, we numerically study the evolution of excess noise in an OPCPA. The observed dynamics explain the macroscopic characteristics seen previously in experiments in the practically important saturation regime.

OCIS codes: (320.7110) Ultrafast nonlinear optics; (230.4480) Optical amplifiers; (190.4970) Parametric oscillators and amplifiers; (030.6600) Statistical optics.

References and links

1. A. Dubietis, G. Jonusauskas, and A. Piskarskas, "Powerful femtosecond pulse generation by chirped and stretched pulse parametric amplification in BBO crystal," Opt. Commun. **88**(4-6), 437–440 (1992).
2. S. Witte, R. Th. Zinkstok, A. L. Wolf, W. Hogervorst, W. Ubachs, and K. S. E. Eikema, "A source of 2 terawatt, 2.7 cycle laser pulses based on noncollinear optical parametric chirped pulse amplification," Opt. Express **14**(18), 8168–8177 (2006).
3. S. Adachi, N. Ishii, T. Kanai, A. Kosuge, J. Itatani, Y. Kobayashi, D. Yoshitomi, K. Torizuka, and S. Watanabe, "5-fs, Multi-mJ, CEP-locked parametric chirped-pulse amplifier pumped by a 450-nm source at 1 kHz," Opt. Express **16**(19), 14341–14352 (2008).
4. D. Herrmann, L. Veisz, R. Tautz, F. Tavella, K. Schmid, V. Pervak, and F. Krausz, "Generation of sub-three-cycle, 16 TW light pulses by using noncollinear optical parametric chirped-pulse amplification," Opt. Lett. **34**(16), 2459–2461 (2009).
5. X. Gu, G. Marcus, Y. Deng, T. Metzger, C. Teisset, N. Ishii, T. Fuji, A. Baltuska, R. Butkus, V. Pervak, H. Ishizuki, T. Taira, T. Kobayashi, R. Kienberger, and F. Krausz, "Generation of carrier-envelope-phase-stable 2-cycle 740-μJ pulses at 2.1-μm carrier wavelength," Opt. Express **17**(1), 62–69 (2009).
6. J. Moses, S.-W. Huang, K.-H. Hong, O. D. Mücke, E. L. Falcão-Filho, A. Benedick, F. Ö. Ilday, A. Dergachev, J. A. Bolger, B. J. Eggleton, and F. X. Kärtner, "Highly stable ultrabroadband mid-IR optical parametric chirped-pulse amplifier optimized for superfluorescence suppression," Opt. Lett. **34**(11), 1639–1641 (2009).
7. O. D. Mücke, S. Ališauskas, A. J. Verhoef, A. Pugžlys, A. Baltuška, V. Smilgevičius, J. Pocius, L. Giniūnas, R. Danielius, and N. Forget, "Self-compression of millijoule 1.5 microm pulses," Opt. Lett. **34**(16), 2498–2500 (2009).
8. E. W. Gaul, M. Martinez, J. Blakeney, A. Jochmann, M. Ringuette, D. Hammond, T. Borger, R. Escamilla, S. Douglas, W. Henderson, G. Dyer, A. Erlandson, R. Cross, J. Caird, C. Ebbers, and T. Ditmire, "Demonstration of a 1.1 petawatt laser based on a hybrid optical parametric chirped pulse amplification/mixed Nd:glass amplifier," Appl. Opt. **49**(9), 1676–1681 (2010).
9. T. T. Ditmire, J. Zweiback, V. P. Yanovsky, T. E. Cowan, G. Hays, and K. B. Wharton, "Nuclear fusion from explosions of femtosecond laser-heated deuterium clusters," Nature **398**(6727), 489–492 (1999).
10. R. A. Snavely, M. H. Key, S. P. Hatchett, T. E. Cowan, M. Roth, T. W. Phillips, M. A. Stoyer, E. A. Henry, T. C. Sangster, M. S. Singh, S. C. Wilks, A. MacKinnon, A. Offenberger, D. M. Pennington, K. Yasuike, A. B. Langdon, B. F. Lasinski, J. Johnson, M. D. Perry, and E. M. Campbell, "Intense high-energy proton beams from Petawatt-laser irradiation of solids," Phys. Rev. Lett. **85**(14), 2945–2948 (2000).
11. W. P. Leemans, B. Nagler, A. J. Gonsalves, C. Tóth, K. Nakamura, C. G. R. Geddes, E. Esarey, C. B. Schroeder, and S. M. Hooker, "GeV electron beams from a centimetre-scale accelerator," Nat. Phys. **2**(10), 696–699 (2006).
12. V. Malka, J. Faure, Y. A. Gauduel, E. Lefebvre, A. Rousse, and K. T. Phuoc, "Principles and applications of compact laser–plasma accelerators," Nat. Phys. **4**(6), 447–453 (2008).
13. F. Krausz and M. Ivanov, "Attosecond physics," Rev. Mod. Phys. **81**(1), 163–234 (2009).

#142105 - $15.00 USD Received 8 Feb 2011; revised 30 Mar 2011; accepted 30 Mar 2011; published 15 Apr 2011

14. S. E. Harris, M. K. Oshman, and R. L. Byer, "Observation of tunable optical parametric fluorescence," Phys. Rev. Lett. **18**(18), 732–734 (1967).
15. C. Dorrer, "Analysis of pump-induced temporal contrast degradation in optical parametric chirped-pulse amplification," J. Opt. Soc. Am. B **24**(12), 3048–3057 (2007).
16. N. Forget, A. Cotel, E. Brambrink, P. Audebert, C. Le Blanc, A. Jullien, O. Albert, and G. Chériaux, "Pump-noise transfer in optical parametric chirped-pulse amplification," Opt. Lett. **30**(21), 2921–2923 (2005).
17. I. N. Ross, P. Matousek, M. Towrie, A. J. Langley, and J. L. Collier, "The prospects for ultrashort pulse duration and ultrahigh intensity using optical parametric chirped pulse amplifiers," Opt. Commun. **144**(1-3), 125–133 (1997).
18. F. Tavella, K. Schmid, N. Ishii, A. Marcinkevičius, L. Veisz, and F. Krausz, "High-dynamic range pulse-contrast measurements of a broadband optical parametric chirped-pulse amplifier," Appl. Phys. B **81**(6), 753–756 (2005).
19. J. Yong-Liang, L. Yu-Xin, Z. Bao-Zhen, W. Cheng, L. Xiao-Yan, L. Hai-He, and X. Zhi-Zhan, "High and stable conversion efficiency obtaining in single-stage multi-crystal optical parametric chirped pulse amplification system," Chin. Phys. Lett. **22**(11), 2840–2842 (2005).
20. F. Tavella, A. Marcinkevicius, and F. Krausz, "Investigation of the superfluorescence and signal amplification in an ultrabroadband multiterawatt optical parametric chirped pulse amplifier system," N. J. Phys. **8**(10), 219 (2006).
21. C. W. Gardner, *Quantum Noise* (Springer-Verlag, 1991).
22. A. Gatti, H. Wiedemann, L. A. Lugiato, I. Marzoli, G.-L. Oppo, and S. M. Barnett, "Langevin treatment of quantum fluctuations and optical patterns in optical parametric oscillators below threshold," Phys. Rev. A **56**(1), 877–897 (1997).
23. J. Chwedeńczuk and W. Wasilewski, "Intensity of parametric fluorescence pumped by ultrashort pulses," Phys. Rev. A **78**(6), 063823 (2008).
24. R. Graham, "Quantum statistics in optics," in *Solid State Physics* (Springer-Verlag, 1973), Vol. 66, pp. 79–81.
25. F. X. Kärtner, R. Schack, and A. Schenzle, "Consistent linearization for quasiprobabilities," J. Mod. Opt. **39**(5), 917–925 (1992).
26. F. X. Kaertner and P. Russer, "Generation of squeezed microwave states by a dc-pumped degenerate parametric Josephson junction oscillator," Phys. Rev. A **42**(9), 5601–5612 (1990).
27. F. X. Kärtner, T. Langer, Ch. Ginzel, and A. Schenzle, "Input-output analysis of nonlinear dissipative quantum systems in the Fokker-Planck approximation," Phys. Rev. A **45**(5), 3228–3241 (1992).
28. P. D. Drummond, "Quantum optical tunneling: A representation-free theory valid near the state-equation turning points," Phys. Rev. A **33**(6), 4462–4464 (1986).
29. P. Kinsler, "Testing quantum mechanics using third-order correlations," Phys. Rev. A **53**(4), 2000–2008 (1996).
30. G. Cirmi, C. Manzoni, D. Brida, S. De Silvestri, and G. Cerullo, "Carrier-envelope phase stable, few-optical-cycle pulses tunable from visible to near IR," J. Opt. Soc. Am. B **25**(7), B62–B69 (2008).
31. C. Manzoni, G. Cirmi, D. Brida, S. De Silvestri, and G. Cerullo, "Optical-parametric-generation process driven by femtosecond pulses: timing and carrier-envelope phase properties," Phys. Rev. A **79**(3), 033818 (2009).
32. S. A. Akhmanov, V. A. Vysloukh, and A. S. Chirkin, *Optics of Femtosecond Laser Pulses* (American Institute of Physics, 1992).
33. Boyd, *Nonlinear Optics*, 3rd ed. (Academic Press, 2008).
34. J. Moses, C. Manzoni, S.-W. Huang, G. Cerullo, and F. X. Kaertner, "Temporal optimization of ultrabroadband high-energy OPCPA," Opt. Express **17**(7), 5540–5555 (2009).
35. F. Haake, H. King, G. Schröder, J. Haus, R. Glauber, and F. Hopf, "Macroscopic quantum fluctuations in superfluorescence," Phys. Rev. Lett. **42**(26), 1740–1743 (1979).

1. Introduction

The optical parametric chirped pulse amplifier (OPCPA) [1] is a ground-breaking tool for intense laser physics. Combining the large gain, broad bandwidth, and high average power handling of an optical parametric amplifier (OPA) with the high-peak-power capability of a chirped-pulse amplifier (CPA), it is currently the most promising technology for scaling the peak power of ultrashort light pulses throughout the visible [2–4] and near-to-mid infrared spectral ranges [5–7]. The technology is essential both for high-energy, petawatt laser facilities [8] used to study laser fusion [9], proton beam emission from solids [10], and compact optical electron acceleration [11,12], and for sources of multi-terawatt carrier-envelope phase stable few-cycle pulses used to control electron wavepacket evolution in atoms and molecules [13].

Like any phase insensitive optical amplifier, OPCPAs are subject to amplified spontaneous emission, often called parametric superfluorescence (PSF), i.e., parametric amplification of the quantum noise due to two-photon emission from a virtual level excited by the pump field and stimulated by the signal and idler field zero-point fluctuations [14]. This process, together with the amplified stimulated emission (ASE) contributions or other intensity fluctuations of the pump laser [15,16], affects the amplified pulse contrast. As we find in this study, the amplification properties of an OPCPA uniquely affect its noise

#142105 - $15.00 USD Received 8 Feb 2011; revised 30 Mar 2011; accepted 30 Mar 2011; published 15 Apr 2011

performance. In a conventional CPA, in which a laser medium amplifies a chirped signal pulse, a population inversion of localized emitters provides homogeneously broadened gain that saturates with the pulse fluence. In contrast, an OPCPA is based on instantaneous second-order nonlinear processes, and the excited virtual levels travel with the pump pulse at a group velocity closely matching that of the signal; the virtual levels therefore saturate instantaneously on the signal's retarded time frame. Compared to a standard OPA, an OPCPA adds the complexity of a map of instantaneous frequency to temporal coordinate during amplification due to the strong linear chirp which allows for inhomogeneous saturation of the available parametric gain.

Experiments have shown that amplification in the presence of PSF in an OPCPA results in an amplified signal field with two macroscopic components showing different energy localization: (i) a coherent pulse with well defined temporal chirp matching that of the injected signal pulse (the "seed") and which therefore can be compressed to generate a Fourier transform-limited pulse; (ii) an incoherent pedestal with phase statistics similar to that of PSF, which remains at picosecond duration when the signal pulse is recompressed [17,18]. Henceforth, we refer to these phenomenological components observed at the output of an OPCPA as the coherent pulse and incoherent pedestal, respectively. Especially in the case of a broadband signal and high gain, a severe impact of PSF on noise performance is also well documented [5,6,19]: it both degrades the signal stability and places an upper limit on the extractable signal energy, due to transfer of pump energy to the incoherent pedestal. The dynamics of this energy transfer during amplification have not been observed yet: their understanding in the highly nonlinear saturation regime is not only of fundamental interest, but is particularly important with regard to performance, since amplifier saturation is necessary for obtaining good conversion efficiency and stable output energy. Intuition, based on the properties of laser and electrical amplifiers, suggests that saturation should suppress fluctuations. However, the effects of saturation on excess quantum noise lack a satisfactory description: while the experiments show degradation of pulse contrast during saturation [6,19], a numerical analysis of output statistics of PSF in an OPCPA seeded by a distributed classical noise source did not isolate the effect [20].

In this paper, we introduce a quantum-mechanically consistent numerical model of the dynamics of PSF growth in an OPCPA that captures the process of energy exchange during amplification between what will become coherent and incoherent components of the electric field after compression, and well reproduces the macroscopic characteristics observed in experiments. Since the purpose of this paper is to isolate the influence of PSF on the amplified pulse contrast, we do not consider effects due to ASE contributions or other intensity fluctuations of the pump laser. By virtue of the model's adherence to quantum mechanics even in the highly nonlinear saturation stage, we observe the saturation dynamics of a quantum-noise-contaminated OPCPA, uncovering several distinguishing features. We find that PSF must be characterized by two observables which display different evolution dynamics: the shot-to-shot energy fluctuation and the ratio of coherent pulse energy and incoherent pedestal energy of the amplified signal field. We find that an OPCPA has well defined but different operating points for maximum suppression of PSF-induced fluctuations or pedestals. Beyond these operating points, heavy saturation leads to large excess noise that can be enhanced by orders of magnitude.

2. Numerical model

For the numerical description of the PSF dynamics in the amplification process, we focus on an OPCPA seeded by the initial quantum noise field and a chirped signal field; amplification occurs in a periodically-poled stoichiometric lithium tantalate (PPSLT) crystal. The nonlinear quantum system dynamics can be described by a quasi-probability distribution, such as the Wigner distribution (WD) [21]. It is well known from quantum optics that for linear systems the evolution equation for the WD is equivalent to a classical Fokker-Planck equation, and is thus also equivalent to a stochastic process involving classical noise sources, resulting in a semiclassical picture of the quantum process. This correspondence has been exploited in

#142105 - $15.00 USD Received 8 Feb 2011; revised 30 Mar 2011; accepted 30 Mar 2011; published 15 Apr 2011

numerical studies of PSF, OPA, and optical parametric oscillation in their linear regimes [22,23]. It is less well known that for the case of weak nonlinearities, i.e., no significant nonlinear effects at the few-photon level, the Fokker-Planck approximation holds and the nonlinear quantum system dynamics can still be extracted accurately from stochastic Langevin equations [24,25], an approach used earlier to study the quantum noise in parametric amplifiers used for squeezed light generation [26,27]. These stochastic equations have a deterministic component equal to the Heisenberg equations of motion for the field operators and are complemented by relaxation terms and associated noise terms. For the case of a lossless OPA process, fluctuations stem solely from the quantum mechanical uncertainty in the input fields. Knowledge of a quasi-probability distribution allows computation of all expectation values of quantum mechanical observables, and for the case of the WD and its associated stochastic process, computed expectation values correspond to quantum mechanical expectation values of symmetrically ordered field operators [21]. Thus, this approach allows for a rigorous treatment of quantum fluctuations in weakly nonlinear quantum optical systems, such as OPCPAs with large mode cross sections. For completeness, we also mention that the quantum dynamics of a second-order nonlinear process, as is the case discussed here, can be described exactly with the help of the positive P-representation, pioneered by Peter Drummond [28]. It has been shown [29] that third- and higher-order moments of the electric field can differ significantly whether calculated by means of the P or truncated WD representation. However, for large normalized photon numbers and weak nonlinearity, differences are very small (the discrepancy was quantitatively small for pump photon numbers of 100 in [25], though some slight differences persisted at early times.). With the gigawatt peak powers typical of OPAs, we are always in the high photon number (totaling ~10^{15} in our case) and weak nonlinearity limit. This fact, together with the increased mathematical complexity of the positive P-representation, using a twice as large phase space which considerably increases computation time, led us to work within the truncated WD.

We simulate the evolution of noise in an OPCPA by numerically solving the coupled nonlinear equations of parametric amplification in the spectral domain, accounting for linear dispersion to all orders [30,31]; the equations describe the interaction among signal, idler and pump, which in the following will be respectively labelled i = 1, 2, 3. These waves propagate along the z coordinate with carrier frequency ω_i and wavenumber k_i. To exploit the large d_{33} nonlinear coefficient of the crystal for all fields polarized along the extraordinary axis, we operate in the quasi phase-matching regime, obtained by periodically poling the nonlinear crystal: poling is accounted for by changing the sign of d_{eff} along z. The carrier fields therefore experience at any crystal coordinate a real phase mismatch $\Delta k = k_3 - k_2 - k_1$. We describe the electric field of each wave as:

$$E_i(z,t) = 1/2 \cdot \left\{ A_i(z,t) \exp\left[j(\omega_i t - k_i z) \right] + \text{c.c.} \right\} = \Re\left\{ A_i(z,t) \exp\left[j(\omega_i t - k_i z) \right] \right\} \quad (1)$$

where $A_i(z,t)$ denotes the field complex amplitude. The coupled equations describing the second order interaction of the fields are derived from the nonlinear propagation equation:

$$\frac{\partial^2 E}{\partial z^2} - \mu_0 \frac{\partial^2 D_L}{\partial t^2} = \mu_0 \frac{\partial^2 P_{NL}}{\partial t^2} \quad (2)$$

applied on the total field $E(z,t) = E_1(z,t) + E_2(z,t) + E_3(z,t)$.

Here $D_L(z,t) = \varepsilon_0 \int \varepsilon_r(\tau) E(z, t-\tau) \mathrm{d}\tau$ is the linear electric induction field accounting for the linear dispersion of the medium [32], and $P_{NL} = 2\varepsilon_0 d_{\text{eff}} E(z,t)^2$ is the nonlinear polarization, where d_{eff} is the effective second-order non-linear coefficient. Since our model also accounts for a broadband noise field, and our purpose is to calculate the evolution of the noise with the highest accuracy, we avoid the slowly-varying-envelope approximation [33] typically adopted to simplify the calculations; in addition we consider the linear dispersion of the material to all orders. For this purpose, we develop Eq. (2) in the frequency domain by taking its Fourier transform and obtaining:

#142105 - $15.00 USD Received 8 Feb 2011; revised 30 Mar 2011; accepted 30 Mar 2011; published 15 Apr 2011

$$\frac{\partial^2 \tilde{E}}{\partial z^2} + \frac{\Omega^2 n(\Omega)^2}{c_0^{\,2}} \tilde{E} = -\mu_0 \Omega^2 \tilde{P}_{NL} \tag{3}$$

where $\tilde{E}(z,\Omega) = \mathcal{F}\{E(z,t)\}$ and $\tilde{P}_{NL}(z,\Omega) = \mathcal{F}\{P_{NL}(z,t)\}$ are the non-unitary Fourier transforms of the electric field and of the nonlinear polarization respectively, Ω is the angular frequency and $n(\Omega)$ is the frequency-dependent refractive index. P_{NL} is developed rejecting components at frequencies different from ω_1, ω_2 and ω_3; when the fields E_i are not overlapped in frequency, wave vector, and polarization, it is possible to split Eq. (3) into three coupled equations which separately describe the evolution of the field envelopes:

$$\begin{aligned}
&\frac{\partial^2 \tilde{A}_1}{\partial z^2} - j2k_1 \frac{\partial \tilde{A}_1}{\partial z} + b_1^{\,2} \tilde{A}_1 = -c_1 \cdot e^{-j\Delta k z} \\
&\frac{\partial^2 \tilde{A}_2}{\partial z^2} - j2k_2 \frac{\partial \tilde{A}_2}{\partial z} + b_2^{\,2} \tilde{A}_2 = -c_2 \cdot e^{-j\Delta k z} \\
&\frac{\partial^2 \tilde{A}_3}{\partial z^2} - j2k_3 \frac{\partial \tilde{A}_3}{\partial z} + b_3^{\,2} \tilde{A}_3 = -c_3 \cdot e^{+j\Delta k z}
\end{aligned} \tag{4}$$

In this case $\tilde{A}_i(z,\omega) = \mathcal{F}\{A_i(z,t)\}$ is the Fourier transform of the envelope amplitude of each field and $\omega = \Omega - \omega_i$ is the detuning from the carrier frequency ω_i; coefficients $b_i^{\,2}$ and c_i are defined as:

$$b_i^{\,2} = -k_i^{\,2} + \tilde{k}_i^{\,2}, \text{ with } \tilde{k}_i = \frac{(\omega+\omega_i)\cdot n_i(\omega+\omega_i)}{c_0} \tag{5a}$$

and

$$\begin{aligned}
c_1 &= \left(\frac{\omega+\omega_1}{c_0}\right)^2 d_{\text{eff}} \mathcal{F}\{A_3 A_2^{\,*}\}, \\
c_2 &= \left(\frac{\omega+\omega_2}{c_0}\right)^2 d_{\text{eff}} \mathcal{F}\{A_3 A_1^{\,*}\}, \\
c_3 &= \left(\frac{\omega+\omega_3}{c_0}\right)^2 d_{\text{eff}} \mathcal{F}\{A_1 A_2\}
\end{aligned} \tag{5b}$$

Here $n_i(\omega + \omega_i)$ are the refractive index functions deduced from the Sellmeier equations, and allow to take into account the whole linear dispersion of the material. The system can be solved as follows: if a suitably small step Δz is chosen, the products $A_3A_2^*$, $A_3A_1^*$ and A_1A_2 are nearly constant, and Eqs. (4) can be analytically solved. Given the fields $\tilde{A}_i(z,\omega)$ at the beginning of a step, the fields at $z + \Delta z$ are:

$$\begin{aligned}
\tilde{A}_1(z+\Delta z,\omega) &\approx \left[\tilde{A}_1(z,\omega) + \frac{c_1}{\gamma_1}\right]\cdot \exp\left[j(k_1-\tilde{k}_1)\Delta z\right] - \frac{c_1}{\gamma_1}\cdot \exp\left[-j\Delta k \Delta z\right] \\
\tilde{A}_2(z+\Delta z,\omega) &\approx \left[\tilde{A}_2(z,\omega) + \frac{c_2}{\gamma_2}\right]\cdot \exp\left[j(k_2-\tilde{k}_2)\Delta z\right] - \frac{c_2}{\gamma_2}\cdot \exp\left[-j\Delta k \Delta z\right] \\
\tilde{A}_3(z+\Delta z,\omega) &\approx \left[\tilde{A}_3(z,\omega) + \frac{c_3}{\gamma_3}\right]\cdot \exp\left[j(k_3-\tilde{k}_3)\Delta z\right] - \frac{c_3}{\gamma_3}\cdot \exp\left[+j\Delta k \Delta z\right]
\end{aligned} \tag{6}$$

where $\gamma_{1,2} = b_{1,2}^{\,2} - \Delta k^2 - 2k_{1,2}\Delta k$ and $\gamma_3 = b_3^{\,2} - \Delta k^2 + 2k_3\Delta k$. It is important to remark that the representation of fields given in Eqs. (4) assumes that pump, signal and idler are three

#142105 - $15.00 USD Received 8 Feb 2011; revised 30 Mar 2011; accepted 30 Mar 2011; published 15 Apr 2011

separate fields. Justifying this treatment, the amplifier we model employs a small non-collinear angle between signal and idler, used both to allow their separation after amplification (since they have opposite temporal chirp) and to avoid signal-idler interference for preservation of carrier-envelope phase of the signal. The results we obtain from our model do not hold for degenerate collinear OPAs, for which fields 1 and 2 of Eqs. (4)–(6) collapse into one equation, and for strongly non-collinear geometries, which would require at least one more spatial coordinate.

Our 1-D plane wave model includes all longitudinal modes, *m*, and their associated noise. In the frequency domain, at any mode frequency, ω_m, the corresponding component of the initial signal, idler, or pump electric field is represented by a complex stochastic phasor, $A_m(0) = B_m + n_m$. B_m is the deterministic component of the field, and is set to 0 in the case of the idler; n_m is a zero-mean, stochastic phasor representing the independent fluctuations of the field.

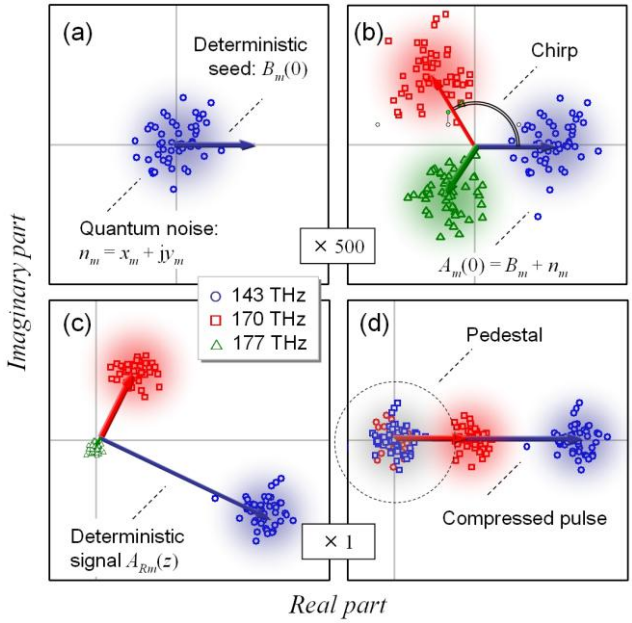

Fig. 1. (Color online) (a) Schematic representation of the deterministic part (arrow) and 50 stochastic components (circles) of a field mode. (b) Initial signal field distribution (scatter), evaluated at three modes of frequency ω_m, experiencing respectively the highest gain G_0, $G_0/2$ and $G_0/10$ and separated by a phase shift imparted by the chirp. (c) Depiction of the same modes after amplification and (d) after compression; pedestal fields deduced after subtracting the deterministic components are indicated in the dashed circle. All data refer to configuration II. Panels (a) and (b) are magnified 500 times with respect to (c) and (d).

Note that fluctuations are included for each of the signal and idler fields; the quantum noise of the pump is negligible, as we also confirmed independently by simulations not reported here. Real and imaginary components of n_m are taken as uncorrelated Gaussian distributions [22] with variance $\sigma_m^2 \propto \omega_m$. A representation of these fluctuating fields is given in Figs. 1(a) and 1(b), where we show B_m (vectors), and A_m and n_m (scatter) for three modes ω_m of the signal field. Our numerical method treats identically the initial electric field components whether originating from the deterministic field or the vacuum fluctuations. We apply this tool to the study of an ultra-broadband OPCPA system known to be sensitive to PSF [5,6]. We model a typical high-gain pre-amplifier, in which noise begins at the vacuum level and that establishes the noise content of later stages of a multi-stage system. The amplifier, pumped by a 9-ps FWHM Gaussian pulse at 1.047 μm and seeded by a broadband (69-THz FWHM) pulse at 2.094 μm for operation around degeneracy, uses a 3-mm long

#142105 - $15.00 USD Received 8 Feb 2011; revised 30 Mar 2011; accepted 30 Mar 2011; published 15 Apr 2011

PPSLT crystal with poling period $\Lambda = 31.2\mu m$. These parameters are close to the experimental conditions of Ref. [6]. The pump-to-seed energy ratio is 10^6.

Table 1. Key Parameter for Three OPCPA Configurations[a]

Config.	Input (z = 0 mm)		Output (z = 3 mm)				
	Seed duration [ps]	Pump intensity [GW/cm^2]	η [%]	Δν [THz]	η·Δν [%·THz]	SPR	SNR
I	1.04	6.254	9.3	**56.8**	528.2	17.1	310.6
II	7.34	8.356	48.5	43.5	**2111.9**	54.2	412.7
III	10.48	8.825	**56.6**	27	1528.2	52.6	322.2

[a]For efficiency η, bandwidth Δν and efficiency-bandwidth product columns, maximum values are highlighted in bold.

The variances σ_m^2 are determined by the quantum fluctuations due to the longitudinal modes of the 100-ps-long simulation window. This number is further increased by a factor equal to the number of transverse modes amplified assuming a pump beam of 100-μm radius in the 3-mm long crystal, which is estimated as about 25. We note that this choice results in a calculated amplified pulse contrast that closely matches that observed in equivalent experiments [6]. This system was investigated previously in order to find the conditions of maximum efficiency-bandwidth product [34]. Following that analysis, we choose 3 values of seed chirp, summarized in Table 1, which correspond to: an under-chirped amplifier, with maximum amplified signal bandwidth but limited conversion efficiency (Configuration I); an amplifier chirped for maximum efficiency-bandwidth product (Configuration II); and an over-chirped amplifier (Configuration III), with excellent conversion efficiency but significant spectral narrowing. Table 1 also provides the pump intensity corresponding to each of the three regimes. For each configuration, we evaluated 50 independent trajectories triggered by uncorrelated noise fields. The averages taken over this ensemble of classical solutions correspond to quantum-mechanical expectation values [35]. The results of a batch of simulations are depicted in Fig. 1(c).

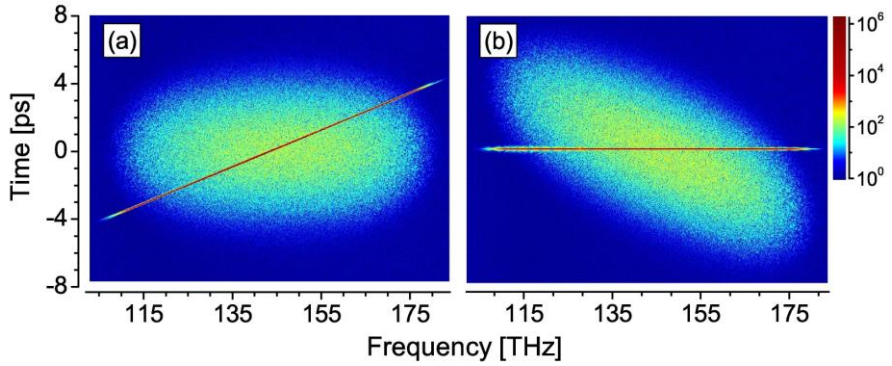

Fig. 2. (Color online) WD map of a signal field from configuration II, evaluated before (a) and after (b) compression.

The incoherent nature of the amplified noise is evidenced in panel (d), representing the same fields after compression. A complete description of an amplified signal field is given in Fig. 2, showing the WD before (a) and after (b) compression. The WDs clearly reveal the presence of a strong incoherent field, arising from PSF, superimposed to the coherent chirped amplified signal; as a feature common to all configurations, this component has a spectrum corresponding to the phase-matching bandwidth of the OPCPA, and duration comparable to

#142105 - $15.00 USD Received 8 Feb 2011; revised 30 Mar 2011; accepted 30 Mar 2011; published 15 Apr 2011

the pump pulse. After applying a linear chirp to compress the coherent pulse (see Fig. 2(b)), the incompressible temporal pedestal degrades the pulse contrast, as observed in experiments.

In addition to this pedestal, PSF also strongly affects the shot-to-shot energy stability of the amplified signal. The noise contaminating the signal field during the OPCPA process can thus be characterized by two quantities: (i) the signal-to-noise ratio (SNR), which evaluates the shot-to-shot energy fluctuation of the signal pulse; (ii) the signal-to-pedestal ratio (SPR), which measures the ratio between the energies of the coherent pulse and the incoherent pedestal. To calculate the SNR we must derive the expectation value and variance of a mode intensity $I_m(z) = a_m\dagger(z)\, a_m(z)$ of signal or idler, (where $a_m\dagger(z)$, $a_m(z)$ are the photon creation and annihilation operators), in terms of expectation values of the classical stochastic field variables $A_m(z)$, $A_m^*(z)$. Equating the computed expectation values of the stochastic field variables to the expectation values of the corresponding symmetrically ordered quantum mechanical field operators, we derive:

$$\langle I_m(z)\rangle = \left\langle |A_m(z)|^2 \right\rangle - \left\langle |n_m|^2 \right\rangle \tag{7a}$$

$$\left[\Delta I_m(z)\right]^2 = \left\langle \left(\Delta |A_m(z)|^2\right)^2 \right\rangle - \left\langle |n_m|^2 \right\rangle^2 \tag{7b}$$

Equations (7) give us a physically satisfying answer for the initial field intensity and variance: $\langle I_m(0)\rangle = |B_m|^2$, *i.e.*, the deterministic component of the initial field, and $\left[\Delta I_m(0)\right]^2 = 2|B_m|^2 \left\langle |n_m|^2 \right\rangle$, *i.e.*, the corresponding photon number fluctuations or shot noise. These equations also correctly give a null expectation value and null variance for a vacuum state ($B_m = 0$): this is of key importance, since the simulation is initially dominated by modes in the vacuum state. From these quantities we can calculate the expectation value $\langle E(z)\rangle$ and variance $\Delta E(z)$ of the pulse energy:

$$E(z) = \sum_m I_m(z)\Delta\omega_m \tag{8a}$$

$$\left[\Delta E(z)\right]^2 = \left\langle (E(z) - \langle E(z)\rangle)^2 \right\rangle \tag{8b}$$

and define $SNR(z) = \langle E(z)\rangle / \Delta E(z)$. Figure 3 shows the evolution with propagation length of $\langle E(z)\rangle$ and $\Delta E(z)$ for signal and idler, while Fig. 4(a) shows *SNR(z)* (solid lines). The pedestal field is deduced from the comparison between the PSF-contaminated signal field $A_m(z)$ and a reference field $A_{Rm}(z)$ obtained from the simulation of a noise-free amplifier ($n_m = 0$). In Figs. 1(c) and 1(d) the dots correspond to the PSF-contaminated signal fields and the arrows to the deterministic reference fields. We find that PSF does not significantly modify the amplification regime, in terms of pump depletion; the pedestal field $A_{Pm}(z)$ can be therefore evaluated as $A_{Pm}(z) = A_m(z) - A_{Rm}(z)$. The SPR is finally evaluated by taking the ratio between the signal and the pedestal pulse energy.

It should be noted that, while the SNR can be measured by the shot-to-shot fluctuations of the amplified pulses, the SPR is difficult to characterize experimentally. In fact, the effect of PSF cannot be isolated by measuring an unseeded OPCPA, since pump depletion is much lower than in the seeded case. The experimental measurement of the evolution of these quantities during the OPCPA process poses an even greater challenge. Our numerical approach, on the other hand, has the unique capability of isolating the pedestal field from the signal under realistic conditions, allowing exploration of its dependence on amplifier parameters, as well as SNR and SPR evolution in the OPCPA crystal.

#142105 - $15.00 USD Received 8 Feb 2011; revised 30 Mar 2011; accepted 30 Mar 2011; published 15 Apr 2011

3. Results and discussion

In Fig. 3 we report the evolution of energy mean and standard deviation of signal and idler, for configurations I and II; for completeness, we have extended the calculation beyond the optimum crystal length of 3 mm. From the curves we can clearly identify three stages of amplification: growth, saturation, and over-saturation.

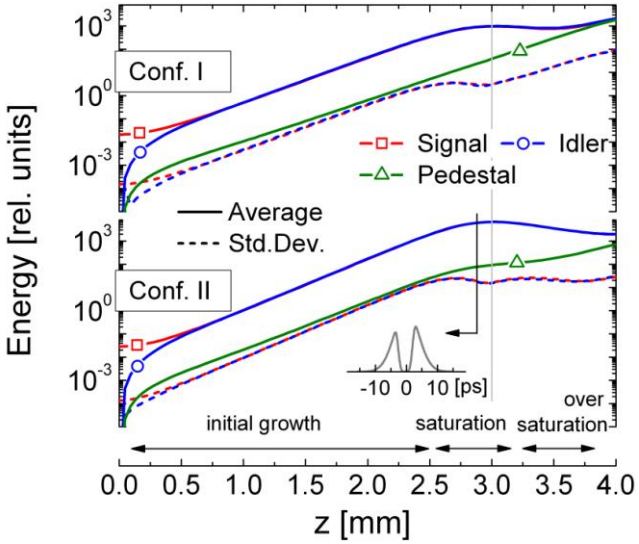

Fig. 3. (Color online) Evolution of energy mean and standard deviation for signal and idler; the energy growth of the pedestal mean is also given. In the case of configuration II we indicate the coordinate at which the pump peak is fully depleted (see inset). Trends calculated for configuration III (not shown) are comparable to the ones of configuration II.

At the start of amplification, the unseeded idler intensity catches up with the signal and the signal standard deviation grows relative to the mean as a result of mixing with the idler, causing a degradation of the initial SNR [Fig. 4(a)]. After this, exponential growth of both waves sets in. In this regime we observe a gradual decay of SNR.

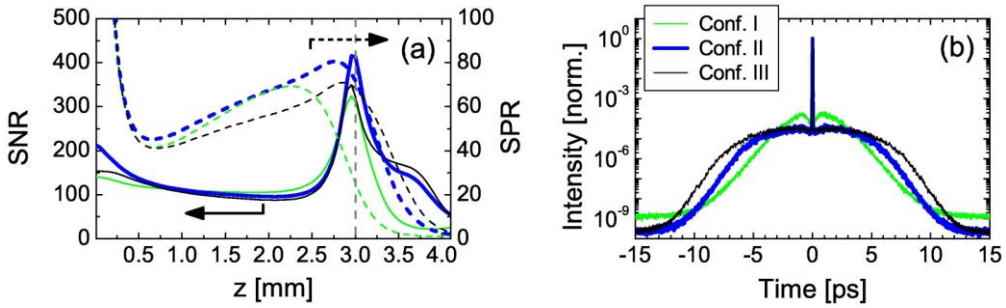

Fig. 4. (Color online) (a) Evolution of SNR and SPR for the three configurations of Table 1. (b) Temporal profiles of the signal pulses after compression, each normalized to its peak.

Once we enter the pump depletion regime, however, the signal energy fluctuation is dramatically reduced, thus improving the SNR. The SNR reaches a sharp maximum shortly before the exit facet of the crystal, close to the propagation distance for which the pump peak fully depletes and the maximum pump to signal/idler conversion occurs. After this point, a rapid drop in SNR is seen. This clearly shows that, while in the pump depletion regime the SNR can be considerably enhanced, in over-saturation the mean intensity sags due to back-conversion to the pump, while noise continues to grow on average across the pulse. Figure

#142105 - $15.00 USD Received 8 Feb 2011; revised 30 Mar 2011; accepted 30 Mar 2011; published 15 Apr 2011

4(a) also shows that, while the three configurations exhibit very similar trends up to saturation, configuration II is preferable due to its higher SNR value.

After saturation, the low-chirp configuration results in the most dramatic drop in SNR, a result of strong growth of PSF in the unseeded temporal wings while the amplified signal converts back to pump at the pulse center. In comparison, the SPR trend reveals dramatic differences with that of SNR, indicating that the energy of the incoherent pedestal, evaluated through the SPR, is not directly correlated to the pulse energy fluctuations measured by the SNR. In fact, maximum suppression of energy fluctuations in configuration I occurs simultaneously with strong degradation of pulse contrast, and in this case the SPR is sharply reduced at the peak of saturation, *i.e.*, at z = 3 mm, where conversion efficiency and efficiency-bandwidth product are maximized. The two parameters therefore offer complementary information for evaluating the impact of excess noise in the OPCPA. The profile of the incoherent pedestal after pulse compression is given in Fig. 4(b); as expected, configuration I is strongly contaminated by an incoherent pedestal generated at unseeded temporal coordinates. Note that the different pedestal durations are due to pulse compression, which imparts a vertical shearing to the WDs (see Fig. 2). These observed dynamics explain the experimental results of Ref. [6], including the non-intuitive result that a saturated amplifier can exhibit reduced pulse contrast. We note, the observed degradation of SPR in saturation, and of both SPR and SNR in oversaturation, are characteristic phenomena singular to quantum noise growth in an OPCPA. In a conventional CPA, there is no oversaturation regime; while nonlinear wave mixing in an OPCPA allows back-conversion of signal and idler to pump after amplification, saturation of a population inversion in a laser is not reversible. Laser gain saturation is also homogeneous, and, therefore, unlike the OPCPA, unseeded frequency modes of the signal field cannot continue to amplify exponentially while the gain for seeded modes saturates. In a conventional OPA, the absence of a chirp ensures that saturation and back-conversion is uniform with respect to frequency, and no macroscopic pedestal is produced, thus allowing SNR to fully characterize the noise performance.

4. Conclusions

In conclusion, we have performed a quantum-mechanically consistent numerical investigation of the dynamics of PSF growth in a realistic high-gain OPCPA. Thanks to the model's capability to simulate also the saturation stage of amplification, this investigation for the first time captures all dynamics of a quantum-noise-contaminated OPCPA, addressing the important practical issues of signal energy stability and pulse contrast. Both quantities are related to the incoherent pedestal superposed to the signal, but display different evolution dynamics throughout the amplification process. Three operating conditions were explored, characterized by different chirps of the input seed and maximizing, respectively, the bandwidth, the efficiency-bandwidth product, and the conversion efficiency. We find that the chirp maximizing the efficiency-bandwidth product is also characterized by the smallest contribution of the noise, both in terms of energy fluctuation and of pulse contrast. Significantly, we find that while amplifier saturation improves the signal's shot-to-shot energy stability, it does not necessarily improve the pulse contrast. In fact, for the case of an amplifier optimized for bandwidth, strong degradation of the pulse contrast (i.e., growth of the PSF-derived incoherent pedestal energy relative to the coherent signal pulse energy) is observed in saturation. Over-saturation, sometimes employed to boost amplifier bandwidth at the expense of conversion efficiency, uniformly reduces both pulse contrast and energy stability.

Knowledge of these dynamics thus provides important insight for the optimization of OPCPA systems applied to the study of strong-field laser physics, as well as increases our fundamental understanding of quantum noise in parametric amplification.

Acknowledgments

This work was partially supported by the U.S. Air Force Office of Scientific Research (AFOSR) under grants FA8655-09-1-3101, FA9550-09-1-0212 and FA9550-10-1-0063, and the Progetto Rocca.

#142105 - $15.00 USD Received 8 Feb 2011; revised 30 Mar 2011; accepted 30 Mar 2011; published 15 Apr 2011

Ultrabroadband pulse generation by coherent synthesis of two optical parametric amplifiers

C. Manzoni[1], S.W. Huang[2], G. Cirmi[2], J. Moses[2], F. X. Kärtner[2,3], and G. Cerullo[1]

[1] *IFN-CNR, Dipartimento di Fisica, Politecnico di Milano, Piazza L. Da Vinci 32, 20133 Milano, Italy*

[2] *Department of Electrical Engineering and Computer Science and Research Laboratory of Electronics, Massachusetts Institute of Technology, Cambridge, Massachusetts 02139, USA*

[3] *DESY-Center for Free-Electron Laser Science and Hamburg University, Notkestraße 85, D-22607 Hamburg, Germany*

cristian.manzoni@polimi.it

Abstract: We present a scheme for the generation of ultrabroadband light pulses based on the coherent synthesis of the pulses delivered by two broadband optical parametric amplifiers. The scheme provides μJ-level pulses with a spectrum ranging from 500 to 1000 nm, supporting sub-4 fs duration. The preliminary results obtained here demonstrate that this scheme is suitable for the generation of single-cycle CEP-stable pulses, whose energy can be boosted by additional amplification stages.

Few-cycle optical pulses are currently used to drive strong-field processes such as high-harmonic generation (HHG), which has recently led to the generation of isolated attosecond pulses as short as 80-as in the XUV range[1]. These processes are sensitive to the electric field of the pulse rather than its envelope profile, thus requiring control of the pulses Carrier-Envelope Phase (CEP) to obtain a reproducible electric field. In addition, a broadband source is necessary to access the few-to-single optical cycle regime. White-light seeded Optical Parametric Amplifiers (OPAs) are powerful tools for the generation of ultrabroadband pulses, since they can provide, under suitable phase-matching conditions, ultrabroad gain bandwidths[2]. In addition OPAs offer the opportunity to produce pulses with passively stabilized CEP, exploiting the difference frequency generation process that occurs in the idler beam synthesis[3]. Broad gain bandwidth in an OPA is achieved when the group velocities of signal and idler are matched[2]; this condition is satisfied either in the case of type I phase matching at degeneracy, or in the non-collinear OPA (NOPA), in which the idler group velocity is projected along the signal propagation direction. Using these concepts, a variety of broadband OPA schemes, pumped by either the fundamental frequency (FF) or the second harmonic (SH) of Ti:Sapphire, have been demonstrated. In particular, 6-fs visible pulses can be routinely generated by SH-pumped NOPA[4], and sub-7-fs pulses are produced in the 650-nm to 950-nm spectral region by the SH-pumped degenerate OPA[5]. Since the WLC presents a highly structured intensity and phase profile around the driving pulse wavelength, for the degenerate OPA additional stages are necessary to shift the WLC driving wavelength to the infrared and to generate well-behaved WLC around 800 nm.

In this work we present a scheme for the generation of CEP-stable (sub)single-cycle pulses in the spectral range from 500 to 1000 nm. The scheme, summarized in the block diagram of Fig. 1, combines (i) the generation of a passively CEP-stabilized WLC seed with (ii) two broadband OPAs seeded by distinct portions of the WLC and (iii) coherent combination of their outputs in order to synthesize high energy (sub)single-cycle pulses with controlled electric field profile.

The system is powered by 550-μJ pulses from an amplified Ti:sapphire laser, providing 100-fs pulses at 800-nm wavelength and 1kHz repetition rate. The first block[5] is a two-stage IR OPA for the generation of high energy IR pulses. When pumped by 250-μJ pulses, this OPA provides a total signal+idler energy of 35 μJ.

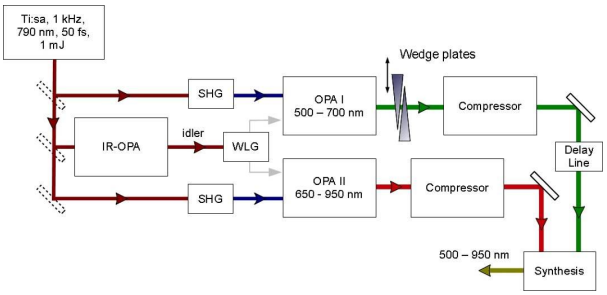

Fig. 1: setup for separate amplification, compression and coherent combination of visible and near-infrared pulses. SHG: second harmonic generation; WLG: white light generation.

Both the signal and the CEP-stable idler can be used to generate a WLC by self-phase-modulation either in a 3-mm thick sapphire plate or in a 4-mm thick YAG respectively. This broadband seed ranges from 500 to 1000 nm, and covers without gaps the amplification range of the subsequent visible NOPA and SH-pumped degenerate OPA (see Fig 2). For the preliminary demonstration of the overall scheme reported here, we tuned the OPA at 1.3 μm and we used its signal beam for WLC generation in sapphire. The supercontinuum is then split by a neutral-density

ultrathin beam-splitter, and the two replicas are amplified by the visible NOPA and by the degenerate OPA. The OPAs are pumped by the SH from the remaining 300-μJ FF pulses; thick SH crystals were used to narrow the bandwidth of the SH pulse, and to facilitate its temporal overlap with the chirped WLC. Each of the two OPAs provides pulses with energy of 1-2 μJ.

To ensure good spatial overlap of the collimated beams, the two OPAs are designed in order to employ the same focal lengths and to propagate the beams for the same distances. Compression is separately achieved by visible and IR chirped mirrors, which shorten the pulse duration close to the transform-limit.

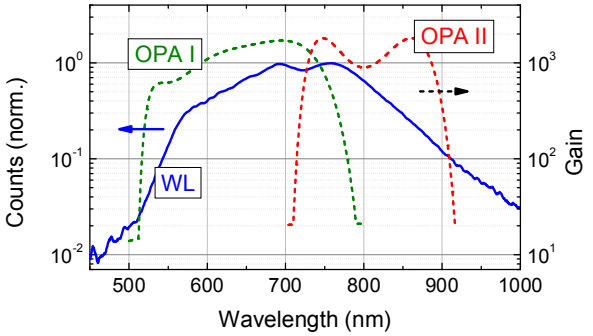

Fig.2: Spectrum of the gap-free supercontinuum (blue solid line) generated in the YAG/sapphire plate, compared to the gain of the visible and infrared OPAs that will be employed for its amplification.

The two amplified pulses are then synchronized by a delay line equipped with a piezoelectric actuator, and collinearly combined by a second ultrathin beam-splitter. A gap-free spectrum arising from the combination of the two pulses is shown in Fig. 3; it supports sub-4 fs pulse duration.

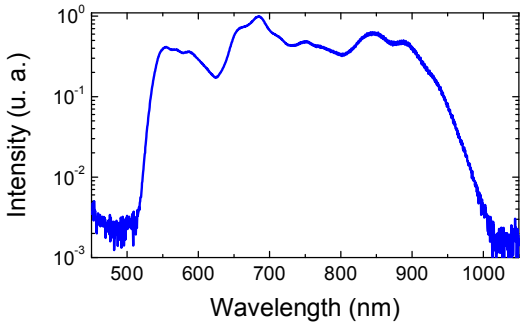

Fig.3: Spectrum of the synthesized pulses; the spectrum supports sub-4 fs pulse duration.

The last challenging step of the pulse synthesis is the coherent combination of the two pulses, which calls for careful control of their relative delay and phase. Thanks to the spectral overlap of the two beams, we could directly use spectral interferometry to characterize their delay fluctuations; for this purpose, the delay between the unlocked pulses was increased to about 200 fs and the spectral fringes were monitored for one minute, giving slow delay fluctuations with rms of the order of 3 fs. When seeded with CEP stable continuua, we plan to lock the relative delay of the pulses by using a balanced nonlinear cross-correlator[6], which allows attosecond-precision relative timing stability thanks to the capability of the balanced detection scheme to cancel the amplitude noise[7]. This scheme, together with the possibility to seed the OPAs with CEP-stable light, will allow the generation of single-cycle pulses with fully controlled electric field. An additional challenge will be full temporal characterization of the synthesized ultrabroadband pulse, which will be performed by two-dimensional spectral-shearing interferometry[8].

REFERENCES

1. E. Goulielmakis, M. Schultze, M. Hofstetter, V. S. Yakovlev, J. Gagnon, M. Uiberacker, A. L. Aquila, E. M. Gullikson, D. T. Attwood, R. Kienberger, F. Krausz, and U. Kleineberg, "Single-Cycle Nonlinear Optics," *Science*, **320**, 1614 (2008).
2. G. Cerullo and S. De Silvestri, "Ultrafast optical parametric amplifiers," *Rev. Sci. Instr.* **74**, 1 (2003).
3. A. Baltuška, T. Fuji, and T. Kobayashi, "Controlling the Carrier-Envelope Phase of Ultrashort Light Pulses with Optical Parametric Amplifiers,"*Phys. Rev. Lett.* **88**, 133901 (2002).
4. T. Wilhelm, J. Piel, and E. Riedle, "Sub-20-fs pulses tunable across the visible from a blue-pumped single-pass noncollinear parametric converter", *Opt. Lett.* **22**, 1494 (1997)
5. A. M. Siddiqui, G. Cirmi, D. Brida, F. X. Kärtner, and G. Cerullo, "Generation of <7 fs pulses at 800 nm from a blue-pumped optical parametric amplifier at degeneracy," *Opt. Lett.* **34**, 3592-3594 (2009)
6. T. R. Schibli et al., "Attosecond active synchronization of passively mode-locked lasers by balanced cross correlation", *Optics Letters* 28, 947-949 (2003).
7. S.-W. Huang, G. Cirmi, J. Moses, K.-H. Hong, S. Bhardwaj1, J. R. Birge, L.-J. Chen, E. Li, B. J. Eggleton, G. Cerullo, and F. X. Kärtner, "Scalable High-Energy Sub-Cycle Waveform Synthesis for Strong-Field Physics", accepted for publication in *Nature Photonics*
8. J.R Birge, H.M. Crespo, and F.X. Kärtner, Theory and design of two-dimensional spectral shearing interferometry for few-cycle pulse measurement", *Journal of the Optical Society of America B,* **27**, 1165-1173 (2010).

Superfluorescence Dynamics of OPCPAs in the Saturation Regime

J. Moses[1], ***C. Manzoni***[2], ***G. Cerullo***[2], ***F. X. Kärtner***[1]

1. Department of Electrical Engineering and Computer Science and Research Laboratory of Electronics, Massachusetts Institute of Technology, Cambridge, MA 02139, USA

2. IFN-CNR Dipartimento di Fisica, Politecnico, Piazza L. da Vinci 32, 20133 Milano, Italy

In the past several years, a new class of ultrashort pulse sources for long-wavelength-driven strong-field experiments has been developed based on ultrabroadband optical parametric chirped pulse amplification (OPCPA) with 2-μm signal wavelength [1-3]. These amplifiers share the advantageous properties of few-cycle duration, passive carrier-envelope phase control and close-to-millijoule energy, but also, due to low seed energy, high gain, and large mode cross section, a propensity towards significant contamination from amplified vacuum noise. This amplified superfluorescence has been found both to degrade the signal-to-noise ratio (SNR) and to transfer a significant portion of the pump wave energy to an incoherent pedestal remaining after compression. The ratio of coherent amplified signal energy and incoherent superfluorescence pedestal energy, *i.e.*, signal-to-pedestal ratio (SPR), has been measured as low as 4:1 [2], and its degradation remains a limitation to pulse energy scalability. Due to the intrinsic difficulty of their experimental measurement and the nonlinear and quantum-mechanical nature of the physical system, the saturation dynamics of quantum noise in OPCPA have remained controversial. Their understanding, however, is requisite for optimization of OPCPA performance.

In this work, we have conducted a numerical analysis of saturation dynamics of quantum-noise contaminated OPCPA employing a new approach which captures the dynamics of energy exchange during amplifier saturation between what will become coherent and incoherent components of the electric field after compression, and well reproduces the macroscopic characteristics observed in experiments upon comparison. Our approach utilizes the correspondence between the evolution equations of quantum mechanical expectation values and the classical Fokker-Planck equations even for nonlinear systems, when the nonlinearity is suitably weak [4]. This allows us to accurately compute quantum-mechanical expectation values from stochastic distributions of a signal and vacuum noise seeded OPCPA system solved numerically from the classical equations of motion.

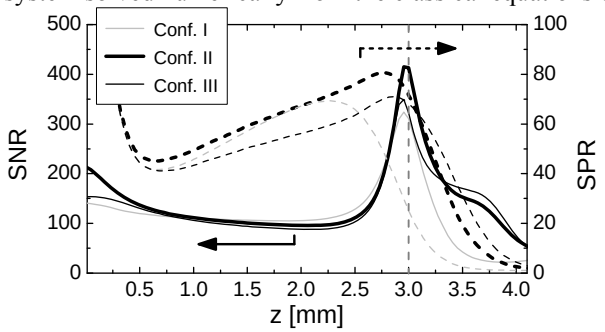

Fig. 1 SNR and SPR versus crystal length for a 2-μm ultra-broadband OPCPA system. Configurations I, II, and III correspond to a system with signal chirp optimized for bandwidth, efficiency, or efficiency-bandwidth product, respectively, as defined in [5]. For all cases, full saturation at the pump pulse peak occurs very near $z = 3$ mm.

We find several distinguishing features. SNR and SPR display different evolution dynamics, and an OPCPA has well defined but different operating points for maximum suppression of noise-induced fluctuations or pedestal. Beyond these operating points heavy saturation leads to large excess noise that can be enhanced by orders-of-magnitude. Comparison of this analysis to a 2-μm amplifier system [3] yields good agreement. In particular, we find that while SNR generally improves during saturation (*i.e.*, shot-to-shot fluctuations are suppressed), the SPR degrades, especially for OPCPA systems with a high degree of saturation and low degree of signal chirp chosen to optimize bandwidth. These observations provide important guidelines for the design and operation of low-noise OPCPAs and insight into the dynamics of quantum noise in a chirped pulse amplifier generally.

References

[1] T. Fuji, N. Ishii, C. Y. Teisset, X. Gu, T. Metzger, A. Baltuška, N. Forget, D. Kaplan, A. Galvanauskas, and F. Krausz, "Parametric amplification of few-cycle carrier-envelope phase-stable pulses at 2.1μm," Opt. Lett. **31**, 1103 (2006).

[2] X. Gu, G. Marcus, Y. Deng, T. Metzger, C. Teisset, N. Ishii, T. Fuji, A. Baltuska, R. Butkus, V. Pervak, H. Ishizuki, T. Taira, T. Kobayashi, R. Kienberger, and F. Krausz.,"Generation of carrier-envelope-phase-stable 2-cycle 740-μJ pulses at 2.1-μm carrier wavelength," Opt. Express **17**, 62 (2009).

[3] J. Moses, S.-W. Huang, K.-H. Hong, O. D. Mücke, E. L. Falcão-Filho, A. Benedick, F. Ö. Ilday, A. Dergachev, J. A. Bolger, B. J. Eggleton, and F. X. Kärtner, "Highly stable ultrabroadband mid-IR optical parametric chirped-pulse amplifier optimized for superfluorescence suppression", Opt. Lett. **34**, 1639 (2009).

[4] F. Kärtner, R. Schack, and A. Schenzle, "Consistent Linearization for Quasi-probabilities," J. Mod. Opt. **39**, 917 (1992).

[5] J. Moses, C. Manzoni, S.-W. Huang, G. Cerullo, and F. X. Kärtner, "Temporal optimization of ultrabroadband high-energy OPCPA," Opt. Express **17**, 5540 (2009).